

1 **Oblique rifting triggered by slab tearing : the case of the Alboran**
2 **rifted margin in the eastern Betics**
3

4 Marine Larrey^{1,2}, Frédéric Mouthereau^{1*}, Damien Do Couto³, Emmanuel Masini⁴, Anthony
5 Jourdon⁵, Sylvain Calassou² and Véronique Mieggebielle²

6 ¹Université Paul Sabatier, Géosciences Environnement Toulouse, GET UMR 5563, Toulouse, France.

7 ²TOTAL S.A., Centre Scientifique & Technique Jean Féger, Pau, France.

8 ³Sorbonne Université, CNRS-INSU, Institut des Sciences de la Terre Paris, ISTeP UMR 7193, F-75005 Paris,
9 France.

10 ⁴M&U sas, France.

11 ⁵Institute of Geophysics, Ludwig-Maximilians-Universität München, Munich, Germany.

12 *Corresponding author:* Frédéric Mouthereau (frederic.mouthereau@get.omp.eu)

13

14 **Abstract**

15 The tectonic evolution of highly oblique continental margins that result from extension above lithospheric STEP faults
16 is poorly understood. Here, we investigate the case of the Alboran margin in the eastern Betics characterized by crustal
17 thinning of 15-10 km, oblique to the direction of slab retreat. The current deformation patterns indicate that oblique
18 rifting is underway. However, it is unclear whether these conditions are those that prevailed during the formation of
19 the metamorphic domes and intramontane basins. We review the temporal and spatial evolution of Neogene
20 sedimentary basins and brittle deformation in the eastern Betics, and exploit offshore seismic reflection lines to
21 propose a crustal-scale section across the oblique margin. The history of sediment infill and rates of subsidence
22 combined with the analyses of fault slip data, confirm that brittle extension oriented from N20°E to EW occurred
23 during an interval spanning from the Serravallian-early Tortonian to the late Tortonian (14-8 Ma). This extension is
24 associated with both normal and strike-slip regimes and the evolution of the strike-slip fault zones flanking the
25 metamorphic domes. The transtensional model forms a coherent scheme linking the ductile deformation associated
26 with metamorphic domes and the formation of EW- and NW-SE/NNW-SSE-directed sedimentary basins in the brittle
27 upper crust during the Tortonian. The oblique extension, which is closely associated with STEP faulting, occurred
28 during the regional convergence between Africa and Iberia since the Miocene. Only recently, around 8 Ma, slab
29 detachment started to migrate westward, leading to tectonic inversion in the eastern Betics. Such a type of narrow
30 oblique rifted margin associated with transform-like plate boundaries is not unique but is expected to be hardly
31 preserved in the geological record due to the transient nature of retreating subduction systems.

32 **1 Introduction**

33 **1.1 Tear faulting and oblique crustal thinning in the Betics**

34 Lithospheric tear faults or subduction-transform edge propagator (STEP) faults are propagating strike-slip faults that
35 accommodate the differential motion between the retreating subduction zone and the overriding plate (Govers and
36 Wortel, 2005). Because of the relative motion between back-arc and surrounding plates, they are also propagating
37 strike-slip faults defined by a sharp contrast in crustal thickness. As noted by Govers and Wortel (2005) such oblique
38 fault boundaries do not necessarily form proper transform plate boundaries but broad zones of distributed deformation,
39 accommodating differential trench-parallel extension, strike-slip motion and rotation. In case the lithospheric tear
40 propagates within the continent-ocean transition, a narrow continental margin forms highly oblique to the direction of
41 back-arc extension. This is documented, for instance, in the Carribean, along the transcurrent Carribean-South
42 America plate boundary (Pindell and Kennan, 2009) or on the margin of the South Orckney microcontinent, along the
43 Scotia-Antarctic plate boundary (Dalziel et al., 2013). Despite the large-scale kinematic picture is relatively well
44 understood, there are only few places on Earth where continental crustal deformation associated with slab-edge
45 continental rift system can be studied both onland and offshore.

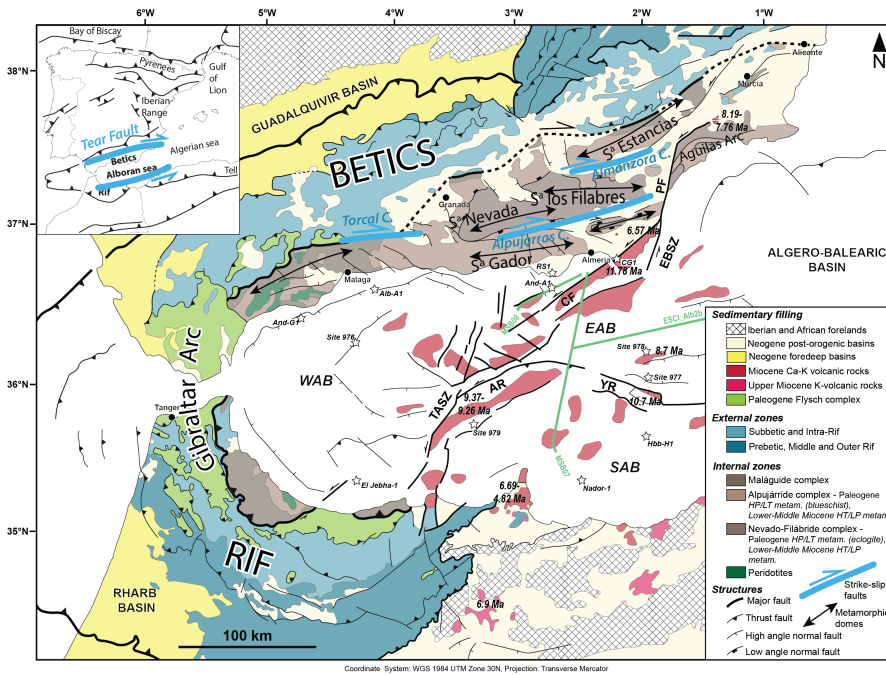
46 Here, we focus on the eastern Betic Cordillera, which constitutes a rifted margin defined by decreasing crustal
47 thickness from >35 km to 20 km onshore (Diaz et al., 2016), thinning offshore to 16-6 km in the Eastern Alboran arc
48 to back-arc region (Booth-Rea et al., 2018; Gómez de la Peña, 2020a) (**Figs 1 and 2**). This region is seen to develop
49 above a EW-trending STEP fault at the boundary between the Alboran basin and the Iberian paleomargin (Badji et
50 al., 2014; Gallais et al., 2013; Jolivet et al., 2021a; Mancilla et al., 2015a). The tectonic expression of the strike-slip
51 deformation during E-W-directed crustal extension above the lithospheric tear is however controversial. On the one
52 hand, low-angle ductile extensional detachments with a top-to-the-west sense of shear are the main features
53 accommodating deformation in the overriding plate. Yet, a-type metamorphic domes in the lower crust, elongated
54 parallel to the E-W direction (**Fig. 1**), formed during the early Miocene, are viewed to express the transtensional
55 deformation at the tip of propagating tear (Lc Pourhiet et al., 2012). On the other hand, E-W-directed transfer strike-
56 slip faulting is interpreted as a late (post-middle Miocene) brittle deformation feature associated with differential E-
57 W crustal extension between the metamorphic domes in the eastern Betics (Alpujarras fault zone ; Sanz de Galdeano
58 and Vera, 1992; Sanz de Galdeano et al., 1985; Martínez-Martínez et al., 2006) and in the western Betics (Torcal fault
59 zone ; Barcos et al., 2015) unrelated to ductile deformation (**Fig. 1**). In line with the latter interpretation, the dextral
60 motion these transfer faults accommodate is assumed to be modest, reflecting a recent post-8 Ma kinematic change
61 that accompanies the stalling of westward slab rollback, the onset of tectonic inversion in the Gibraltar Arc (Do Couto
62 et al., 2014; d'Acremont et al., 2020; Jolivet et al., 2021a; Martínez-García et al., 2017), and progressive slab tearing
63 and delamination of the lithospheric mantle from the eastern to the central Betics (Martínez-Martínez et al., 2006 ;
64 Mancilla et al., 2015a ; García-Castellanos and Villaseñor, 2011; Spakman et al., 2018). Note that in a recent study
65 the dextral displacement since 9 Ma has been estimated to more than 100 km along the Torcal fault (Crespo-Blanc et
66 al., 2016).

67 The lack of structural, temporal constraints and quantification of belt-parallel motion along these faults indicates,
68 however, that we do not yet fully understand their link with the long-term evolution of slab tearing and margin

Deleted: the formation of
Formatted: Normal, Justified, Line spacing: 1,5 lines
Formatted: Font: Bold, English (US)
Deleted: rifted margin
Formatted: Font: Bold
Formatted: Font: Bold
Formatted: Font: Bold
Formatted: Font: Bold

71 formation. For instance, the current deformation patterns in the Central Betics, where metamorphic domes are present,
 72 brings evidence that both strike-slip faulting and extension operate synchronously (Martínez-Martínez et al., 2006).
 73 This is shown by the west-directed GPS velocities increasing westwards indicating ongoing extension, and the west-
 74 directed displacements increasing from North to South, towards the Alboran domain, revealing right-lateral shear (Fig.
 75 2). This together with evidence for present-day 4.5 mm/yr westward displacement and rotations in the Western Betics
 76 and Rif reveal that the westward slab rollback is likely to be still ongoing (Fadil et al., 2006; Gonzalez-Castillo et al.,
 77 2015). The current transtensional deformation across the Betic Cordillera is consistent with the current stress regime
 78 defined by extension direction highly oblique (max. 20°) to the Betic structural trend (or 70° spanned by the direction
 79 of extension and normal of the rift trend).

Deleted: rollback



80
 81 **Figure 1** : Geological map of the Betic-Rif arc. Main tectonic units and age of volcanism as well as major structures
 82 and Neogene sedimentary basins are shown. The studied offshore seismic lines (red) is displayed as well as offshore
 83 wells and ODP sites (open star) for stratigraphic calibration in the East (EAB), South (SAB) and West Alboran basins
 84 (WAB). CF: Carboneras Fault; PF : Palomares Fault; AR: Alboran Ridge; YR: Yusuf Ridge; EBSZ : East Betic Shear
 85 Zone; TASZ: Trans-Alboran Shear Zone.

Moved (insertion) [1]

Moved (insertion) [2]

Formatted: Font colour: Text 1, English (US)

88 **1.2 Highly oblique rifting triggered by slab tearing : a proof of concept in the eastern Betics**
89 Right-lateral transtensional deformation in the Betics agrees with the extrusion model of the Alboran basin towards
90 the Gibraltar arc to the West (Borque et al., 2019; Palano et al., 2015) caused by indentation by the east Alboran
91 domain likely enhanced by resistance slab dragging (Spakman et al., 2018). In the East, the extrusion is accommodated
92 by left-lateral strike-slip displacement along the Eastern Betic Shear Zone (EBSZ; Borque et al., 2019), shaped by the
93 Carboneras Fault (CF) and Palomares Fault (PF), which separates the extrusion domain were extension and
94 transtension is prevailing from the Águilas Arc where N-S indentation is well documented (Ercilla et al., 2022). In
95 this region, this fault extends offshore, across the Alboran Sea, in the larger Trans-Alboran Shear Zone (De Larouzière
96 et al., 1988; Stich et al., 2006) moving at ~4 mm/yr, equivalent to the regional 5 mm/yr NW-directed convergence
97 between Africa (Nubia) and Europe (Fig. 2; Echeverría et al., 2013; Koulali et al., 2011; Nocquet, 2012; Palano et al.,
98 2015, 2013; Vernant et al., 2010). Here, we hypothesize that the present-day oblique extension patterns is at play since
99 the Miocene and explain the formation of the narrow Alboran rifted margin.
100 Only recently high-resolution 3D numerical models have been able to predict the deep structure of oblique rift
101 domains. These models can be used as a guide to re-evaluate the evolution of the Betics. 3D models by Jourdon et al.
102 (2021) predict that oblique extension results in narrow rifted margins, strike-slip faults and corridors coupled with
103 subsident pull-apart basins, normal faults and block rotations (Fig. 3). The recognition of block rotation in the Betic
104 arc (Crespo-Blanc et al., 2016; Platzman, 1992), strike-slip fault zones (Fig. 1) and NW-SE normal faulting, which
105 defines extension direction highly oblique to the margin (Galindo-Zaldivar et al., 2003; Figs 1 and 2), support this
106 view. The simulations also show that the deeper ductile crust experiences thinning (vertical flattening) and stretching
107 perpendicular to the strike of the margin in accordance with stretching lineations parallel to the metamorphic domes
108 and low-angle detachments (Fig. 3). Other types of 3D numerical experiments show that sediment loading of strike-
109 slip faults can result in asymmetric flexural basin with apparent normal fault throw (Neuharth et al., 2021) that can be
110 mistakenly interpreted as resulting from orthogonal extension. Asymmetric basins are indeed intriguing characteristics
111 of intramontane basins in the Betics (Rodríguez-Fernández et al., 2011; Augier et al., 2013; Do Couto et al., 2014 ;
112 Giaconia et al., 2014). Although primarily found associated with divergent plate boundaries e.g. in the Gulf of
113 California (Fossen et al., 2013; Fossen and Tikoff, 1998) highly oblique extension is also documented in active
114 transform regions along the San Andreas Fault (Teyssier and Tikoff, 1998) or the North Anatolian Fault in Marmara
115 Sea (Okay et al., 2004). A detailed analysis of highly oblique rifting deformation in the Gulf of California recognises
116 similar tectonic elements as for the Betics, such as extensional detachment systems orthogonal to the divergence and
117 upper crustal folds trending parallel to the divergence (Fossen et al., 2013).

Deleted:

Deleted: further

Deleted: as a consequence of

Deleted: This

Deleted:

Deleted: ¶ ... [1]

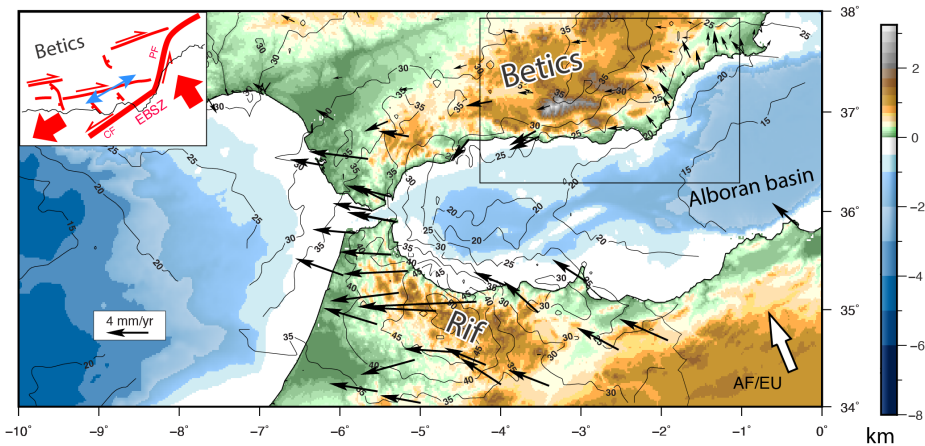
Moved up [1]: Figure 1 : Geological map of the Betic-Rif arc. Main tectonic units and age of volcanism as well as major structures and Neogene sedimentary basins are shown.

Deleted: The studied offshore seismic lines (red) is displayed as well as offshore wells and ODP sites (★) for stratigraphic calibration in the East (EAB), South (SAB) and West Alboran basins (WAB). ...

Moved up [2]: CF: Carboneras Fault; PF : Palomares Fault; AR: Alboran Ridge; YR: Yusuf Ridge; EBSZ : East Betic Shear Zone; TASZ: Trans-Alboran Shear Zone. ¶

Formatted: Font colour: Text 1, English (US)

Deleted:



138

139

140

141

142

143

144

145

146

147

Figure 2 : Present-day kinematics in the Betic-Rif arc and eastern Betic Cordillera (inset). GNSS-based displacements in the western Alboran block and north-western Africa shown in a fixed Eurasian reference frame (black arrows after Palano et al., 2015) are oblique to the AF/EU plate convergence (white arrow) inferred from plate tectonic Morvel model (Argus et al., 2011). Labelled contours depict the crustal depth given in kilometers as inferred from deep seismic profiles and receiver functions analysis (Diaz et al., 2016). In the eastern Betic (inset), W-directed stretching is taken up by EW-directed right-lateral strike-slip fault and NW-SE normal faults. Extension direction resolved from focal mechanisms (blue arrow) are after (Stich et al., 2006). CF: Carboneras Fault; PF : Palomares Fault; AR: Alboran Ridge; YR: Yusuf Ridge; EBSZ : East Betic Shear Zone; TASZ: Trans-Alboran Shear Zone.

Deleted: arrows

148

149

150

151

152

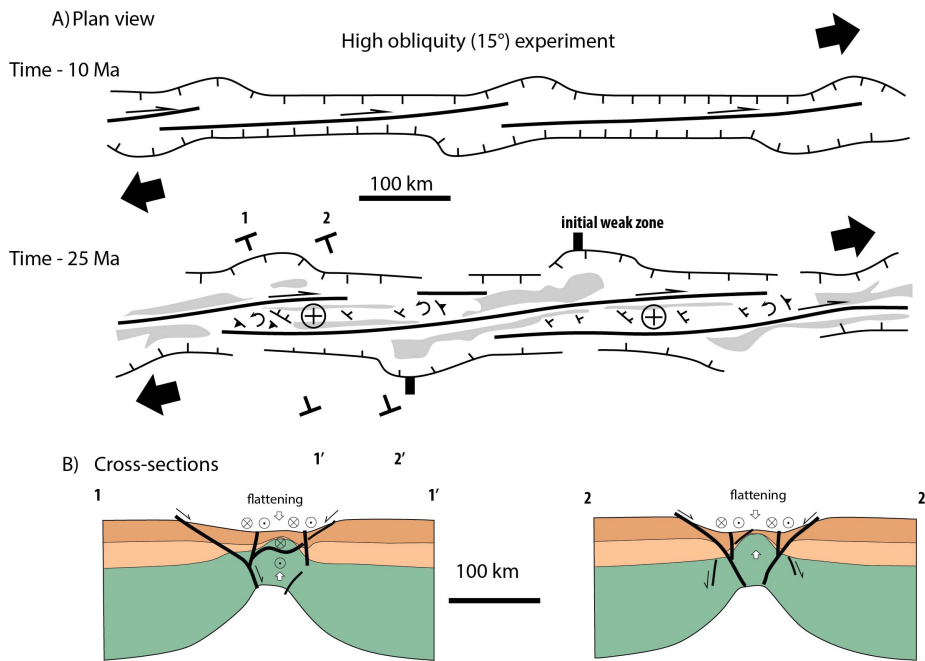
153

154

155

Several tectonic features need further discussion however. First, the relevance of strike-slip faulting in the past is debatable as only a few occurrence of crustal-scale strike-slip faults are mapped (Fig. 1). Second, the detail of the temporal and spatial relationships between the formation of the oblique/transform margin and STEP faulting remain elusive. We here review the temporal and spatial evolution of Neogene intramontane sedimentary basins and related brittle deformation in the eastern Betics. In addition, we exploit offshore seismic reflection lines to propose a new crustal-scale section across the oblique margin. Based on these constraints we present a tectonic scenario for the formation of the high-obliquity rifted margin controlled by STEP faulting.

Deleted: .



158

159 **Figure 3** : Sketch of highly oblique rift experiments based on the results of a 3D thermo-mechanical model (Jourdon
 160 et al., 2021). Results are depicted in plan view (A) and cross-sections (B) for two steps (after 10 Myrs and 24 Myrs)
 161 for the case where extension is set with an angle of 15° with respect to the rift axis. Grey regions in (A) are basins
 162 adjacent to uplifted domains (cross-circle symbol) associated with right-lateral strike-slip faults. Cross-sections (B)
 163 depict the abrupt crustal thinning that occur perpendicular. Crustal thinning is most visible for the lower crust and
 164 produces the formation of an abrupt necking domain controlled by rift-parallel normal faults dipping towards the
 165 center of the rift and right-lateral strike-slip faults.
 166

167 2. Geodynamics and STEP faulting in the Betics

168 The onset of N-directed movement of Africa, by the Late Cretaceous-Paleogene, led to far-field, Laramide-like
 169 contraction from Morocco throughout Western Europe (Mouthereau et al., 2021). South of Iberia, in the Betic-Rif
 170 domain, the closure of hyper-extended rift systems and oceanic basins of the Atlantic-Alpine Tethys resulted in the
 171 development of a proto-Betic accretionary prism, likely largely submerged (Angrand and Mouthereau, 2021; Daudet
 172 et al., 2020; Vergés and Fernández, 2012). By about 50 Ma, the acceleration of plate convergence led to the shortening
 173 of continental rift and oceanic basins and topographic uplift all over Iberia (Daudet et al., 2020; Mouthereau et al.,
 174 2021, 2014; Rat et al., 2019; Vacherat et al., 2016; Waldner et al., 2021) associated with the onset of continental rifting
 175 along the Western European Rift (e.g. Mouthereau et al., 2021). 35 Ma ago, as Africa convergence slowed down, the
 176 western Mediterranean sea opened accompanied by retreating slabs (Dewey, 1988; Dewey et al., 1989; Faccenna et
 177 al., 2014; Jolivet and Faccenna, 2000; Rosenbaum et al., 2002). Subduction occurred mainly before 30 Ma as argued
 178 by age constraints on high-pressure mineral assemblages (Augier et al., 2005a; Bessièrè et al., 2021; Booth-Rea et al.,

~~Deleted~~: showing two steps (after 10 Myrs and 24 Myrs)

~~Deleted~~: of oblique rifting

~~Deleted~~:). Results are redrawn after (Jourdon et al., 2021

~~Formatted~~: Font colour: Auto, English (US)

~~Deleted~~: of a highly oblique experiment

~~Deleted~~: associated

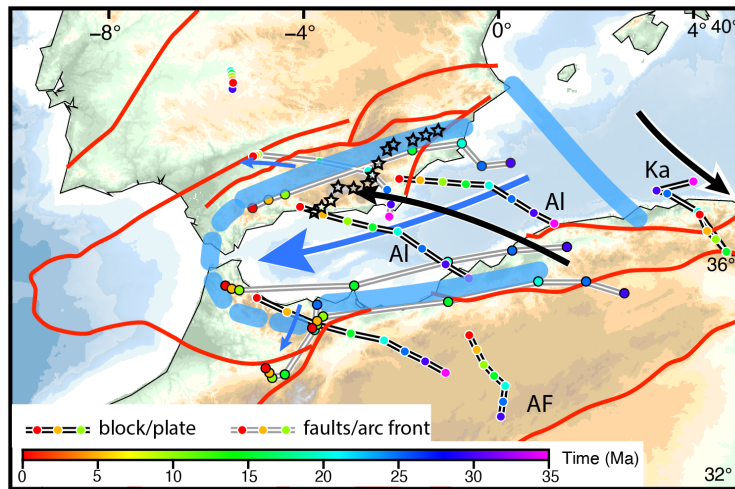
184 2015; Gomez-Pugnaire and Fernandez-Soler, 1987; Platt and Vissers, 1989; Platt and Whitehouse, 1999) and has been
185 suggested to last until the mid-Miocene in the eastern Betics e.g. (Platt et al., 2013). The timing of formation of the
186 Alboran basin is constrained to 23 to 16 Ma by the oldest deposits found on Alboran basement and by the timing of
187 high-temperature metamorphic overprint and rapid cooling to shallow crustal temperature (Bessi re et al., 2021;
188 Daudet et al., 2020; Janowski et al., 2017; Johnson et al., 1997; Platt et al., 2005; Sosson et al., 1998; V zquez et al.,
189 2011; Zeck et al., 1992). The eastern Alboran basin formed later, mostly by late Miocene arc magmatism (Booth-Rea
190 et al., 2007; 2018; G mez de la Pe a et al., 2020a).

191 All kinematic reconstructions agree that extension results from the westward migration of the arc front and retreat of
192 the Alboran slab, well imaged below the Gibraltar arc as a steeply-dipping high-velocity anomaly (Bezada et al., 2013;
193 Heit et al., 2017; Mancilla et al., 2018, 2015a, 2015b; Palomeras et al., 2014; Spakman and Wortel, 2004; Villase or
194 et al., 2015). These reconstructions, however, differ according to the paleo-position of Alboran terrane, and hence to
195 the amount and vergence of subduction (Angrand and Mouthereau, 2021; van Hinsbergen et al., 2014; Lonergan and
196 White, 1997; Romagny et al., 2020; Rosenbaum et al., 2002; Verg s and Fern ndez, 2012). Seismic tomography
197 reveals that slab detachment and tearing occur along the conjugate Alboran margins of the southern Betics and
198 northern Africa (Govers and Wortel, 2005; Heit et al., 2017; Mancilla et al., 2015a; Meighan et al., 2013; Spakman
199 and Wortel, 2004).

200 In **Fig. 4** we refer to the reconstruction of Angrand and Mouthereau (2021) that has the advantage of reconciling
201 previous western Mediterranean models (Romagny et al., 2020; Verg s & Fern ndez, 2012) with recent
202 thermochronological analyses in western Betics (Daudet et al., 2020) and other geological data (see compilation in
203 Mouthereau et al., 2021). This model considers that the Alboran domain has been rifted from Iberia during the Jurassic.
204 It is in agreement with detrital and igneous zircon U-Pb ages that suggest Alboran was attached to Iberia in the late
205 Paleozoic (Jabaloy-S nchez et al., 2021). It also accounts for the existence of an upper Cretaceous-Paleogene foreland
206 basin that formed adjacent to a proto-Betic orogen and in continuity eastwards with the Balearic Promontory. In that
207 respect, it contrasts with other models placing the Alboran domain to the south of the Balearic Promontory (Moragues
208 et al., 2021; van Hinsbergen et al., 2014).

209 In this reconstruction about 400 km of slab retreat is estimated since about 35 Ma (gray path, blue arrows in **Fig. 4**).
210 It is worth noting that for Romagny et al. (2020) a similar amount (i.e. 400 km) is accommodated by back-arc extension
211 of the Alboran crust, implying the same magnitude of displacement along the STEP fault in the Betics. In the
212 reconstruction of Angrand and Mouthereau (2021), however, crustal thinning in Alboran basin is linked to
213 delamination retreat of the Alboran lithospheric mantle towards the west. Because of the decoupling between crust
214 and mantle, the length of the delaminated slab resolved at depth in seismic tomography, should not be simply translated
215 into the amount of E-W crustal extension in the Alboran domain. This further implies that the displacement across the
216 STEP fault must be also less than 400 km. Daudet et al. (2020) suggested that an extension of 110 km estimated from
217 the restoration of low-angle detachment systems in the central and eastern Betics (Martinez-Martinez et al., 2002) is
218 likely to be a more accurate crustal estimate of the movement Alboran domain rather than the total slab length.

219



220
221
222
223
224
225
226
227
228
229

Figure 4: Kinematics of African plate (AF), Alboran (Al) and Kabyliides (Ka) blocks with respect to fixed European plate since 35 Ma reconstructed after Angrand and Mouthereau (2021). Thick blue lines depicts the approximate position of lithospheric tear faults (between Al and Europe and Africa) and transfer faults (between Al and Ka). Tear faults located in Betics and Rif are after Jolivet et al. (2021b). Black stars depicts the positioned of tear fault in the Betics as defined by Mancilla et al. (2015a). Black arrows indicate the movement of Al and Ka with respect to Europe along black motion paths presented from 35 Ma to present. Grey motion paths refer to the motion of specific structures relative to Europe, including the motion of the arc front (thick blue dashed line) and faults in red. Dark blue arrow depicts the movement of the arc front due to retreating delamination towards the west.

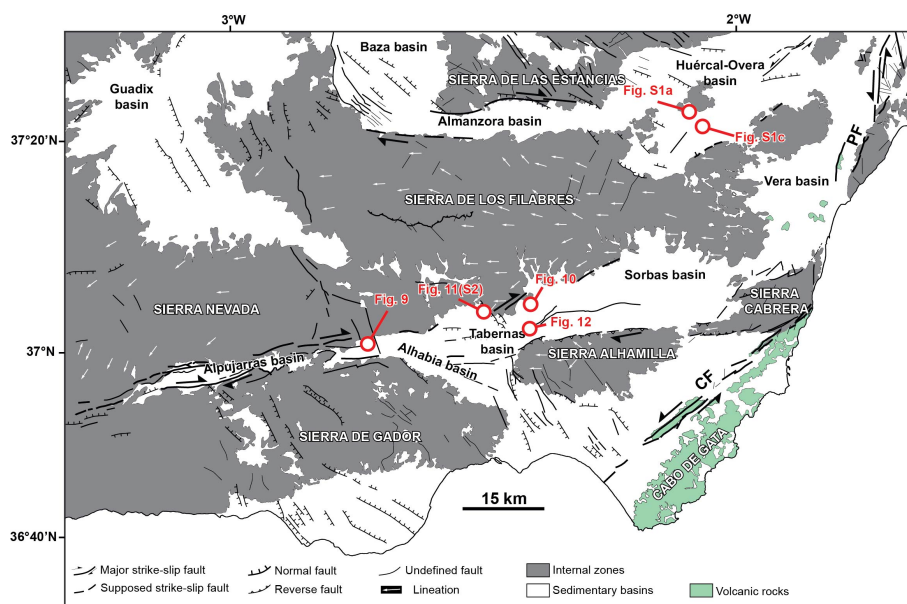
230 3. Miocene extension in the eastern Betics

231 3.1 Relationships between domes and basins : from transtension and pure extension to late tectonic inversion

232 The most prominent extensional features in the eastern Betics are : 1) E-W elongated ranges that formed metamorphic
233 domes with foliations bearing prominent E-W stretching lineations, for instance, in the Nevado-Filabrides
234 Complex (Fig. 5; e.g. Sierra de los Filabres, Sierra Nevada, and the Sierra de las Estancias) and Serravallian-Tortonian
235 sedimentary basins (Tabernas-Sorbas, Alpujarras, Almanzora and Huércal-Overa basins); 2) NNW-SSE/NW-SE
236 normal fault systems and basins oblique to the domes such as the NW-SE trending Guadix-Baza and Alhabia basins
237 (Galindo-Zaldivar et al., 2003; Martínez-Martínez and Azañón, 1997) (Fig. 5). They are described as asymmetric half
238 grabens (Do Couto et al., 2014; Martínez-Martos et al., 2017; Pedrera et al., 2010, 2009) formed during the Upper
239 Serravallian-Early Tortonian (Augier et al., 2005b; Augier et al., 2013; Meijninger and Vissers, 2006). Several of
240 these NW-SE faults are active and cut across the metamorphic domes and the sedimentary basins (Augier et al., 2005a;
241 Booth-Rea et al., 2004a; Giaconia et al., 2012; Montenat and Ott d'Estevou, 1999).

242 In addition to these structures, there are E-W right-lateral strike-slip fault zones and parallel depressions, like the
243 Alpujarras fault zone between the Sierra de Gádor and the Sierra Nevada, and the Almanzora fault zone between the
244 Sierra de los Filabres and Sierra de las Estancias (Fig. 5). The left-lateral Carboneras and Palomares fault system

245 (Reicherter and Hübscher, 2006; Scotney et al., 2000) marks the tectonic limit with the Cabo de Gata volcanic province
 246 (Fig. 5).
 247 The domes are extension-related features interpreted either as 1) EW-metamorphic domes resulting from the
 248 exhumation in the footwall of a regional W-directed extensional low-angle detachments, later folded during post-
 249 Tortonian N-S contraction (Martínez-Martínez and Azañón, 1997; Martínez-Martínez et al., 2002, 2004) or 2)
 250 Miocene metamorphic domes formed by constrictional ductile strain regime accompanying W-directed stretching of
 251 the Alboran domain and trench retreat, with limited overprint by the Tortonian contraction ca. 8 Ma (Augier et al.,
 252 2013; Augier et al., 2005; Augier et al., 2005b; Galindo-Zaldivar et al., 2015; Jolivet et al., 2021b; Martínez-Martínez
 253 et al., 2002). Low-temperature constraints from the Nevado-Filabride and Alpujarride complexes confirm the west-
 254 directed exhumation of the basement that occurred progressively from the Sierra de los Filabres at ~13-11 Ma
 255 (Serravallian) in the East to the Sierra Nevada at 8-6 Ma (Late Tortonian-Messinian) in the West (Clark and Dempster,
 256 2009; Janowski et al., 2017; Johnson et al., 1997; Platt et al., 2005; Reinhardt et al., 2007; Vázquez et al., 2011).
 257



258
 259 **Figure 5** : Tectonic map of the eastern Betics showing the main structural elements in black after Augier et al. (2005)
 260 and Do Couto (2014). CF: Carboneras Fault; PF : Palomares Fault.
 261

262 Tectonic models for the formation of Neogene intramontane sedimentary basins vary depending on the prevailing
 263 tectonic regime. EW-directed basins have been early described as pull-apart basins (e.g Alpujarran fault zone; Sanz
 264 de Galdeano et al., 1985). Structural analyses then led to re-interpret these structures as transfer zones resulting from
 265 differential extension between exhuming core-complexes (and detachment systems) since the Serravallian (13-11 Ma)

266 later refolded during Tortonian (9-8 Ma) compression in the Eastern Betics while extension is still active in the Central
267 Betics (Martínez-Martínez et al., 2006). Other authors proposed that NE-SW extension lasted until 7.5-7 Ma in the
268 Eastern Betics (Booth-Rea et al., 2004b; Giaconia et al., 2014).

269 In support to the compressional stress regime in the Eastern Betics, Martínez-Martos et al. (2017) interpreted the E-
270 W depressions are related to the tectonic reactivation of crustal weakness zone as dextral strike-slip faults in a
271 counterclockwise rotation, accommodating part of the the N-S shortening. There are evidence that at the end of the
272 Tortonian a regional uplift occurred, rising the remnants of late Tortonian marine platform, 7.2 Ma in age, to 1600 m
273 above sea level in the Sierra de Gádor (Braga et al., 2003; Janowski et al., 2017), coincidently with the onset of
274 contraction in the Sierra Alhamilla and Sierra de los Filabres (e.g. Do Couto et al., 2014), in the Alboran domain (e.g.
275 Martínez-García et al., 2017) and on the margins of the eastern Betic (Giaconia et al., 2013 ; 2015). In addition to
276 shortening, this recent uplift may reflect deep mantle mechanisms like slab tearing or delamination (e.g. Duggen et
277 al., 2003; García-Castellanos and Villaseñor, 2011; Mancilla et al., 2015a).

278 Based on the prevalence in some EW-trending basins, like the Huércal-Overa basin, of EW-trending normal faults,
279 these basins have alternatively been interpreted as resulting from late exhumation stage of the domes, possibly as soon
280 as the Serravallian, but mostly after the early Tortonian (syn-sedimentary faulting) (Augier et al., 2013; Augier et al.,
281 2005b; Meijninger and Vissers, 2006). The NW-SE/NNW-SSE sedimentary basins (Guadix, Baza, Alhabia; **Fig. 5**),
282 in contrast, are extensional basins formed parallel to the direction of the regional compression (Sanz de Galdeano and
283 Vera, 1992; Larouzière et al., 1988). E-W strike-slip fault zones, aligned in the direction of the domes, and NW-SE
284 normal faulting patterns are both key features consistent with predictions from models of oblique extension at
285 transform margin (**Fig. 3**). Yet, based on existing structural and tectonic syntheses a clear temporal relationships
286 between E-W ductile stretching in the domes and transcurrent deformation is not established (**Fig. 5**).

287

288 **3.2 Is the Tortonian rift-related subsidence consistent with oblique extension ?**

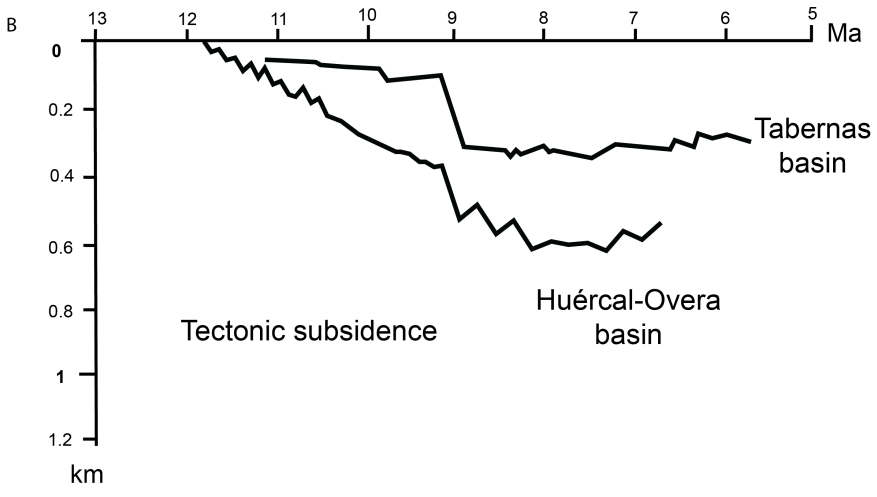
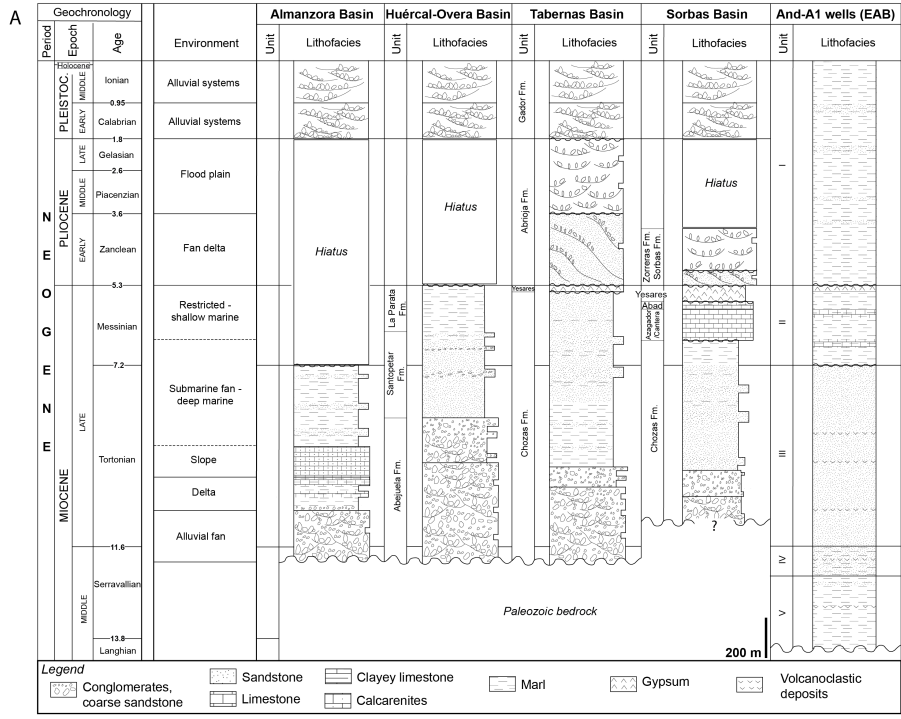
289 The stratigraphic architecture and depositional evolution of Tortonian intramontane basins provides first-order
290 informations on the distribution of crustal thinning. Among the oldest sediments deposited unconformably on the
291 Paleozoic-Triassic basement are the red alluvial conglomerates and deltaic series dated from the Serravallian to the
292 Lower Tortonian (**Fig. 6a**). They are thicker and well exposed on the flanks of the Almanzora basin and on the northern
293 Huércal-Overa basin (HOB), compared to the Alpujarras Corridor (AC) and Tabernas basin (TB) (**Figs. 6 and 7a**;
294 Augier et al., 2013; Pedrera et al., 2010, 2007; Poisson et al., 1996). In the east of the Sorbas basin, it should be noted
295 that Langhian-Serravalian deposits and perhaps sediments as old as Burdigalian have been locally reported (Giaconia
296 et al., 2014).

297 Paleogeographic reconstructions indicate that these Serravallian to Lower Tortonian sediments were deposited on a
298 large emerged domain, stretching from Huercal-Overa to Granada, in the West and in Tabernas, to the South (Braga
299 et al., 2003). Sourced from the Nevado-Filabride metamorphic complex (Hodgson and Haughton, 2004; Kleverlaan,
300 1989; Meijninger and Vissers, 2006; Pedrera et al., 2010, 2007; Pickering et al., 2001; Weijermars et al., 1985) these
301 deposits mark the onset of surface exhumation of the Sierra de Las Estancias and Sierra de Los Filabres.

302 During this initial stage, HOB is the most subsident basin (**Figs. 6b, 7a and 7b**), accumulating sediments at rates of
303 400 m/Ma while rates are 140-180 m/Ma in the Tabernas basin (**Fig. 6b**) (Augier, 2005). Higher subsidence in the
304 HOB, which also started earlier than in other basins, suggests extension occurred originally to the North associated
305 with the exhumation of the Sierra de Las Estancias. Basal continental conglomerates are overlain by grey coarse-
306 grained Tortonian sandstones found occasionally, e.g. in the Almanzora basin, intercalated with marine marls (**Figure**
307 **6a**). They are topped by mid-Tortonian bioclastic calcarenite and coral reefs (Braga et al., 2003; Martin et al., 1989;
308 Pedrera et al., 2007).

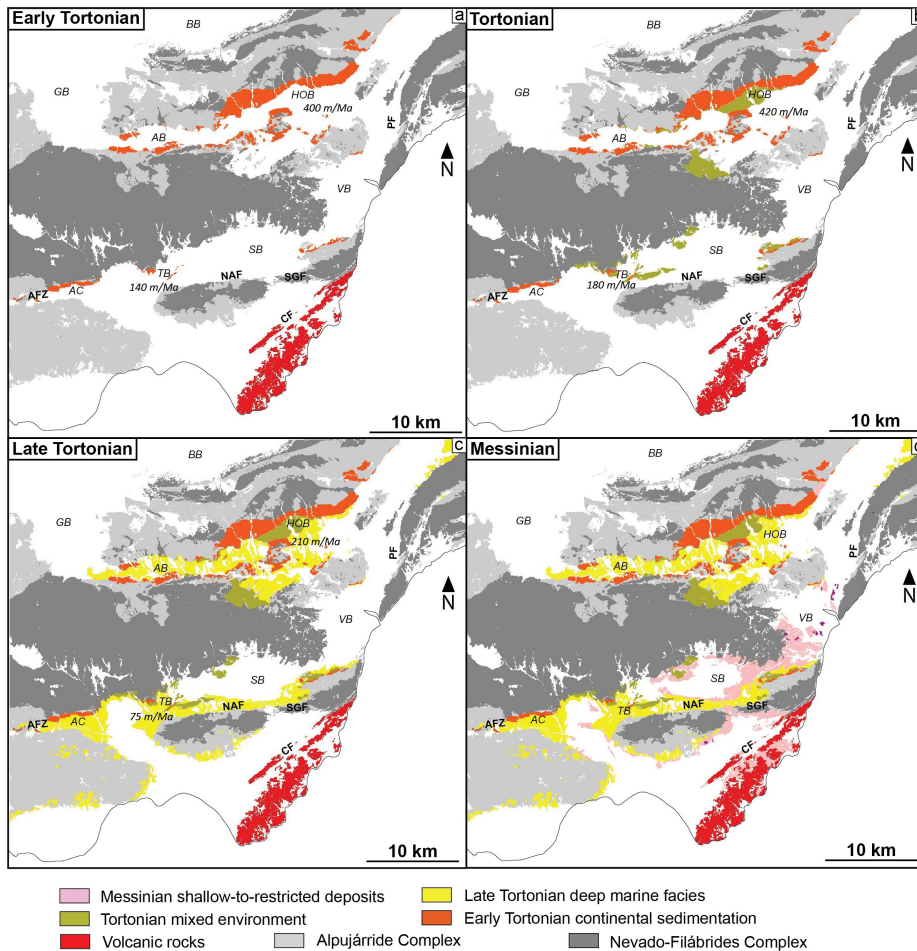
309 During the same interval, TB recorded the deposition of 300 to 400 m of coarse to medium-grained deltaic marine
310 clastics overlying unconformably the lowermost red series (**Fig. 6a**). These sediments pass upwards, e.g. in TB, to
311 deeper marine 1200 m-thick turbiditic and marls series intercalated with regional-scale megabeds, revealing the onset
312 of rapid tectonic subsidence (Haughton, 1994; Kleverlaan, 1989, 1987; Pickering et al., 2001; Weijermars et al., 1985).
313 Details of depositional architecture of the Tortonian suggest that part of this subsidence evolution was controlled by
314 E-W dextral strike-slip faults (Haughton, 2000 ; Baudouy et al., 2021) under transtensional strain.

315 The transition from continental to deep marine sedimentary environments (water depth of 400-600 m according to
316 Poisson et al., 1999) witnesses the rapid rift-related tectonic subsidence achieved during the upper Tortonian times
317 (~9 Ma; **Figs. 6 and 7c**) (Augier et al., 2005b; Montenat and Ott d'Estevou, 1992; Weijermars et al., 1985). At around
318 8 Ma, accumulation rates drop by a factor of two to 200 m/Ma in HOB and 70 m/Ma in TB, revealing a marked
319 reduction in subsidence. Subsidence then became negative as basement uplifted from around 7 Ma (**Figs. 6b and 7d**)
320 in both TB and HOB.
321
322



324 **Figure 6** : Stratigraphic evolution and lithologies of intramontane basins in the eastern Betics and offshore A1 well.
325 (a) Neogene stratigraphy and basin-fill correlation in the Almanzora and Huércal-Overa basins (Mora, 1993), Tabernas
326 basin (Hodgson and Haughton, 2004; Kleverlaan, 1989; Pickering et al., 2001) and Sorbas basin (Fortuin and
327 Krijgsman, 2003; Martin and Braga, 1994; Riding et al., 1998). Middle Miocene sedimentary environments in the
328 Alboran Sea are after (Comas et al., 1992). (b) Neogene tectonic subsidence evolution for Tabernas basin and Huércal-
329 Overa basin are from Augier (2004). The curves are obtained from backstripping techniques incorporating eustatic
330 and paleobathymetric corrections. Question mark beneath the Sorbas basin lithofacies column indicates the potential
331 for uncertainty/variability across the basin (see text).
332

333 The geometry of the Almanzora (Pedrera et al., 2009), Sorbas (e.g. Do Couto et al., 2014) and Huércal-Overa basin
334 basins (Pedrera et al., 2010) inferred from gravity measurements indicate that these basins are asymmetrical and
335 deepening southwards. This sediment infill pattern recalls the formation of asymmetrical basins predicted by
336 numerical models of flexural strike-slip basins (Neuharth et al., 2021). According to this model, the asymmetry
337 observed should reflect the development of strike-slip basins loaded by sediments originated from the North. In
338 addition, a larger subsidence in HOB is an indication of abrupt crustal thinning to the south of Sierra de las Estancias
339 where the crustal thickness is the largest (**Fig. 2**). Therefore, at least the Serravallian-Tortonian infill patterns agree
340 with oblique extension.
341



342
 343 **Figure 7:** Distribution of (a) lower Tortonian, (b) Tortonian, (c) upper Tortonian and (d) Messinian deposits based on
 344 geological mapping of the different basins. CF: Carboneras Fault; PF : Palomares Fault; SGF: South Gafarillo fault;
 345 NAF: North Alhambilla fault; AFZ: Alpujarras fault zone; BB: Baza basin; GB: Guadix basin; AB: Almanzora basin;
 346 HOB: Huercal-Overa basin; VB: Vera basin; SB: Sorbas basin; TB: Tabernas basin; AC: Alpujarras Corridor.
 347

348 **4. Brittle faulting : pure extension versus transtensional deformation in Neogene basins**

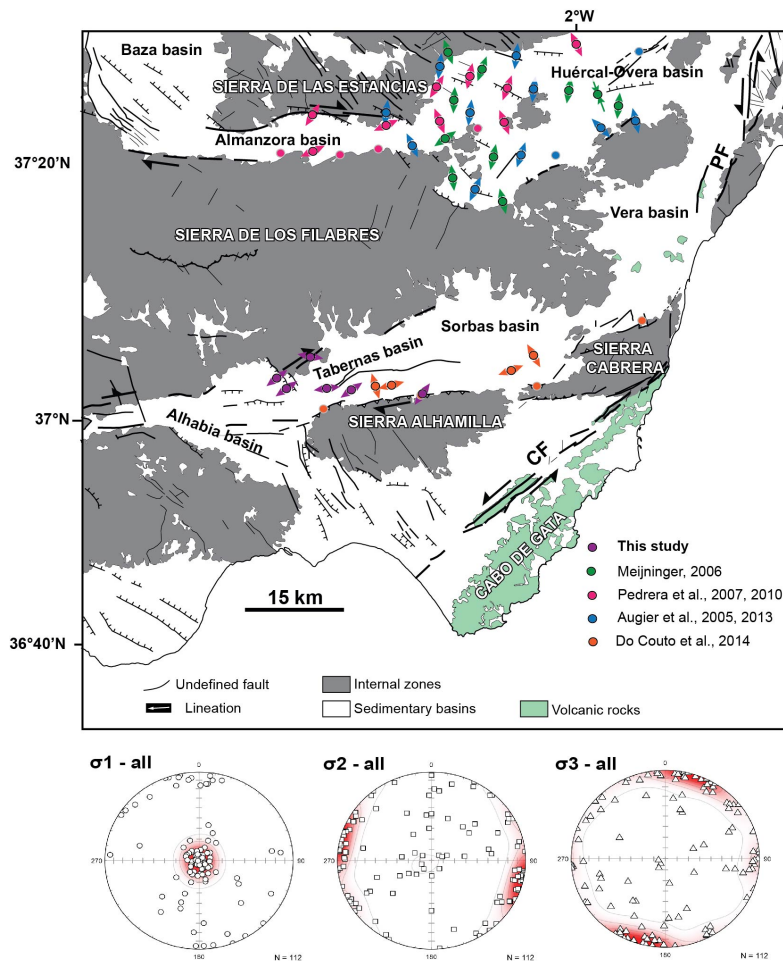
349 **4.1. Tectonic regime in the eastern Betics**

350 **Figure 8** presents a compilation of 112 fault slip data inversion previously analysed in the eastern Betics combined
 351 with new measurements conducted in the Alpujarras Corridor and in the Tabernas basin (**Table S1**). Most faults are
 352 syn-Tortonian or cut through the Tortonian. This compilation emphasizes a regional trend of σ_3 stress axes oriented

353 NNE-SSW (N20°E) with subordinate σ_3 oriented E-W. In details, this well-defined regional horizontal extension
354 reflects a combination of pure normal faulting regime (σ_2 horizontal and oriented NW-SE/WNW-ESE, 73% of stress
355 tensors) and strike-slip faulting regime (σ_2 vertical to steeply-dipping and σ_1 horizontal an striking NNW-SSE, 27%
356 of stress tensors). N-S to NW-SE compression is also reported in the HOB associated with incipient synform and
357 depocenter which is dated to the lower Tortonian coeval with the prominent EW/WSW-ENE extension (e.g. Pedrera
358 et al., 2010).

359 We describe below, based on a selection of outcrops in the vicinity of the contact between Tortonian basins and major
360 metamorphic domes, the expression of EW and NW-SE extensional faulting in the field. We then discuss how they
361 are linked to the regional stress regimes.

362



363
364
365
366
367
368
369
370

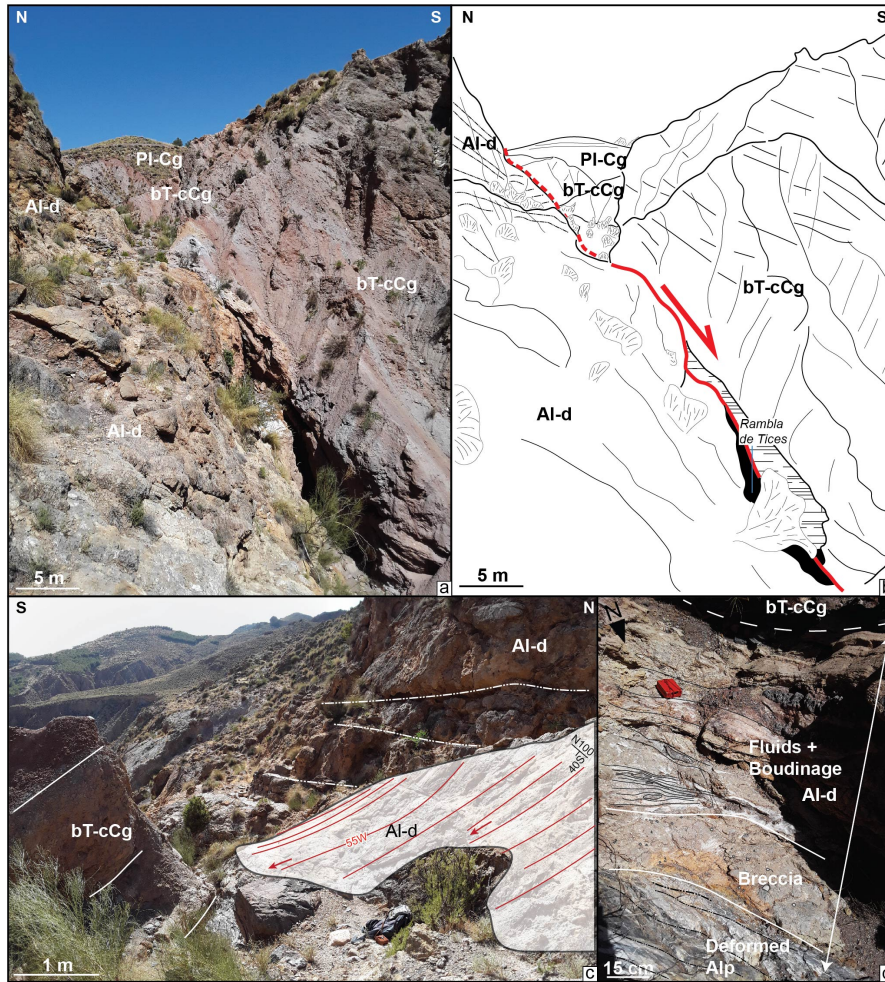
Figure 8: Synthesis of stress regimes resolved from fault slip data inversion in Tortonian basins. Color-coded circles with arrows depict tectonic sites where extension (given as arrows) is horizontal (pure extensional or strike-slip stress regimes). Sites where reverse tectonic regimes prevail are shown as circles highlighted in grey. Below, stereoplots of paleostresses σ_1 , σ_2 and σ_3 show a compilation of all brittle tectonic regimes extracted from Table S1. Collectively they define a prominent extension oriented NNE-SSW with a subordinate E-W-striking extension. CF: Carboneras Fault; PF: Palomares Fault.

371 **4.2 EW-trending faults: evidence for pre-Tortonian oblique extension ?**

372 In Tortonian intramontane basins, one of the main set of faults is represented by E-W-directed faults, including ENE-
373 WSW to ESE-WNW sets. North of the Alpujarras Corridor (AC), 3 km to the NE of Canjáyar, the contact between
374 the basal Tortonian conglomerates and the series of Alpujarride complex is exposed in the Rambla de Tices. It is

Deleted: 1

376 shaped by a 2-meter thick fault zone (**Figs. 9a,b**) striking N100°E, which has a normal sense of slip with a right-lateral
377 strike-slip component (**Fig. 9c**). It consists of cataclastic breccias and sheared blocks (boudins) of the host rocks (**Fig.**
378 **9d**). This major fault is found along the 65 km-long Alpujarras fault zone described by Martínez-Martínez (2006) as
379 a major strike-slip dextral transfer zone south of the Sierra Nevada that accommodates both WSW-extension and dextral
380 movement. It is mechanically consistent with NE-SW/ENE-WSW extension under a strike-slip regime as resolved
381 nearby along the same faults system (Martínez-Martínez, 2006). **Fig. 9** indicates the fault is parallel to the basal
382 Tortonian series but cuts across the Alpujarride complex. In the HOB, on the southern flank of the Sierra Limaria
383 (**Fig. 8**), the unconformity between the lower Tortonian red conglomerates and the Alpujarride units (Rambla de
384 Cordoba, 2km NW Arboleas, **Figs. S1a, b**) is found reactivated as a normal fault with a dextral shear component.
385 To the North of TB, a large morphological surface presents a rare exposure of the micaschist basement of the Nevado-
386 Filabrides complex allowing the study of deformation on the southern flank of the Sierra de los Filabres (**Fig. 10**). The
387 deformed NF series shapes a kilometric-size antiform with axial planar surface dipping towards the North. The steeply-
388 dipping cleavages directed NE-SW on its southern flank are deformed by numerous dextral shear zones with lengths
389 ranging from 100 m to less than 5 m (**Fig. 10b, c**). In addition to isoclinal folds parallel to the main foliation that are
390 clearly associated to an early stage of ductile EW-stretching, we recognize close to the strike-slip shear zones, steeply-
391 dipping metric-size open to tight folds inclined to the NE (**Fig. 10d**). To the south, Tortonian conglomerates are
392 overlying unconformably the folded NF foliation. This stratigraphic relationships and the average low dip of Tortonian
393 strata (20°SE) indicate that strike-slip deformation occurred before the deposition of Tortonian conglomerates and
394 after the tilting of the NF foliation (see cross section in **Fig. 10a**). This argues that the transition from HP
395 metamorphism (Burdigalian-Langhian) in the NF (Platt et al., 2006) to W-directed ductile crustal thinning and right-
396 lateral strike-slip faulting occurred before the Tortonian, most likley around the Serravallian at 12-13 Ma. This interval
397 is considered to mark the transition from ductile to brittle extension in the region (e.g. Augier et al., 2013). Because
398 strike-slip faulting postdates folding of the NF foliation, and are consistent with WSW-ENE oblique extension, we
399 suggest that the Sierra de los Filabres metamorphic dome formed in a transtensional strain regime. This hypothesis
400 conforms with prediction of transtension at the tip of the STEP fault (Le Pourhiet et al., 2012) and with model of
401 oblique extension (see **Fig. 3**).
402



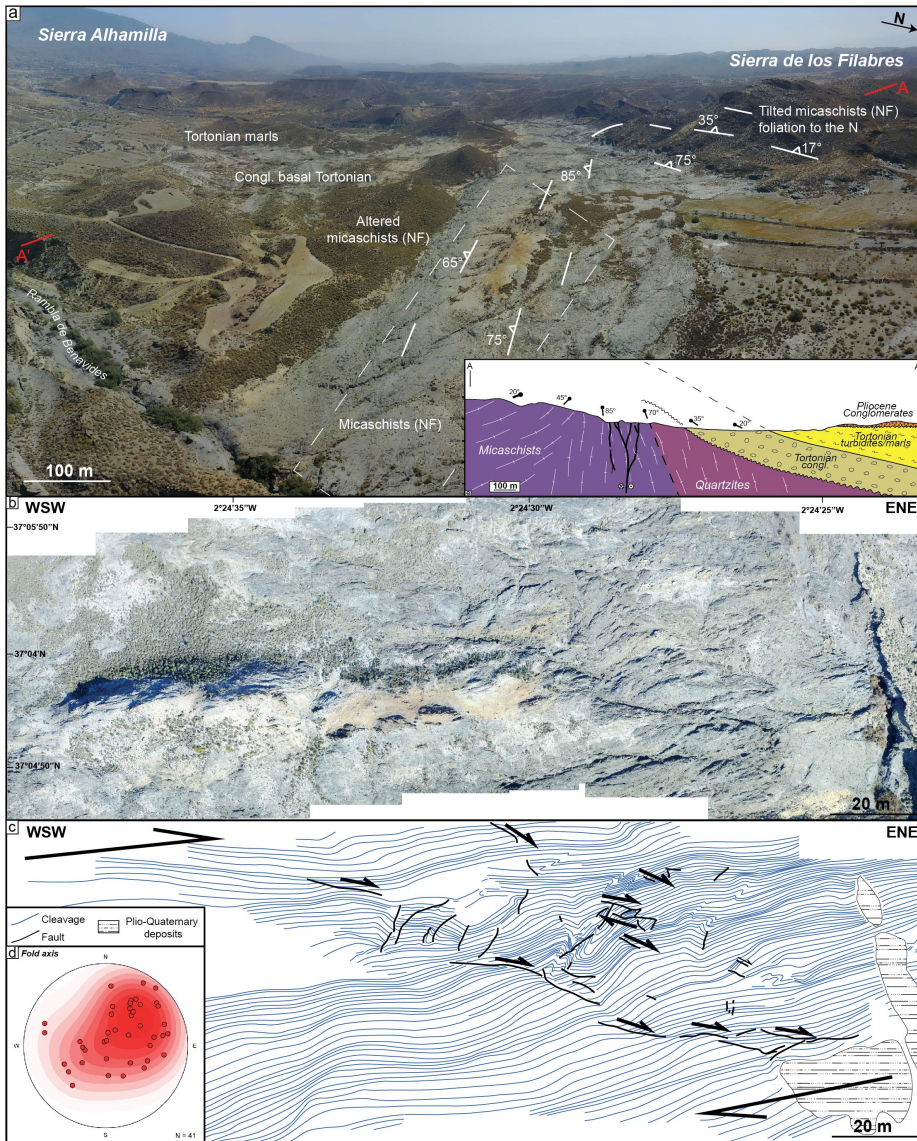
403
 404 **Figure 9.** (a) and (b) Fault zone at the contact between the Tortonian basal conglomerates and the series of the
 405 Alpujarride complex south of AC (Rambla de Tices, see Fig. 5 for location). (c) slickensides on the fault zone reveal
 406 a normal sense of slip with right-lateral strike-slip component found in association with (d) cataclastic breccias,
 407 sheared boudins of metamorphic and sedimentary rocks. Al-d: Alpujarride dolomites; bT-cCg: basal Tortonian
 408 continental Conglomerates; PI-Cg: Pliocene Conglomerates. Coordinates 37.031944°N/-2.716274°E.
 409

410 **4.3. NW-SE-trending normal faults**

411 A second set is represented by NW-SE directed normal faults (Fig. 8). They are found, for instance, bordering the
 412 NE part of Alhabia basin, where they cut across the basement and interrupt the westward continuity of the southern

Deleted: 1.2

414 flank of the Sierra de los Filabres. One major fault zone of this system is well exposed in the Arroyo del Verdelecho,
415 7 km to the west of Tabernas, on the eastern border of the Alhabia basin (**Figs. 11 and S2**). From a regional point of
416 view this large NW-SE fault zone controls the deepening of the Tortonian basin and the position of Pliocene
417 depocenter in its hangingwall, towards the West. NW-SE normal faults also cut across the lower Tortonian
418 conglomerates in the hangingwall but their throw diminishes upward in the upper Tortonian margin sediments,
419 suggesting fault activity during the late Tortonian (**Fig. 11**). One major fault zone is outlined by cataclastic breccias
420 made of marbles originated from the exhumed Alpujarride complex in the Sierra de los Filabres (**Fig. S2**).
421 South of HOB (south of Arboleas), NW-SE faults are seen cutting through the late Tortonian sands and marls series,
422 indicating that NE-SW extension is at least Tortonian (**Figs. S1c, d**).
423



424

425

426

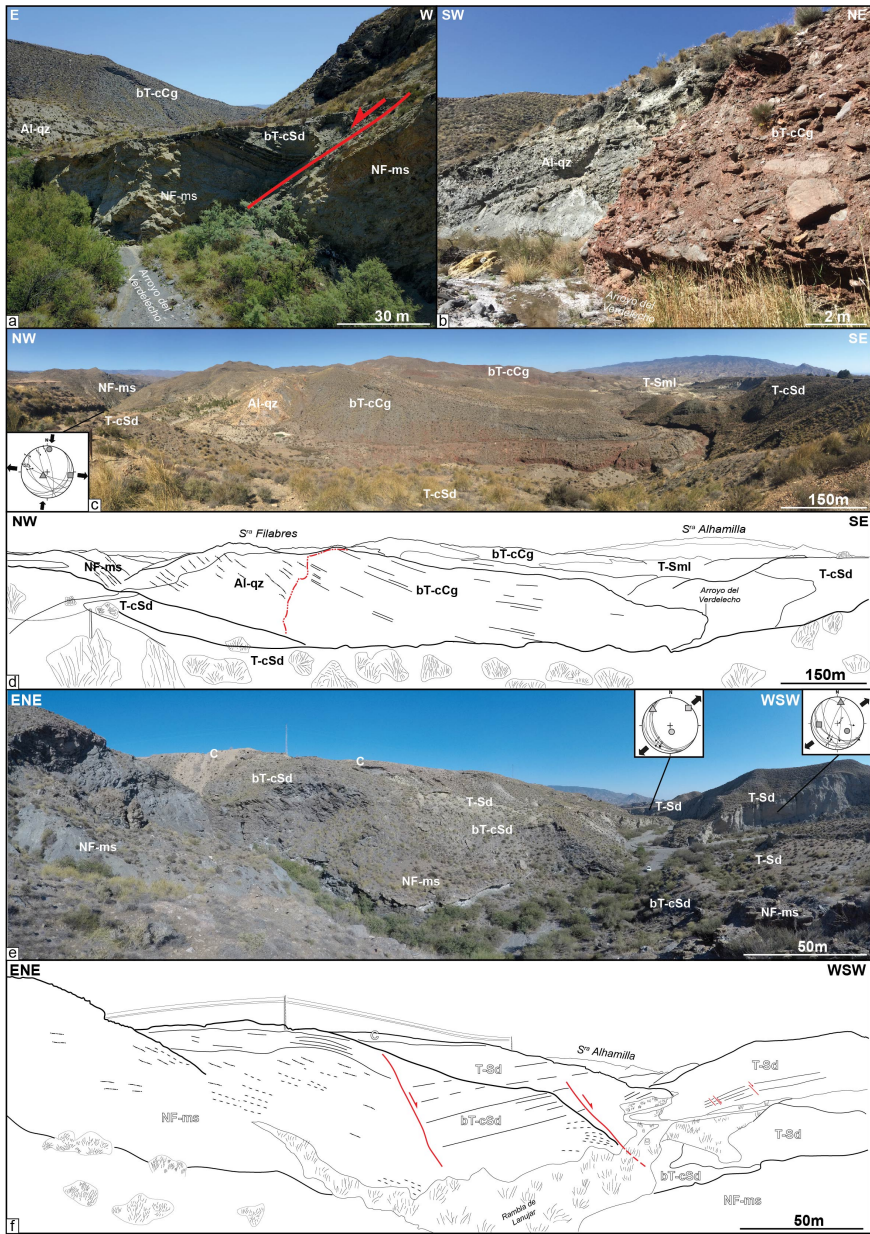
427

428

429

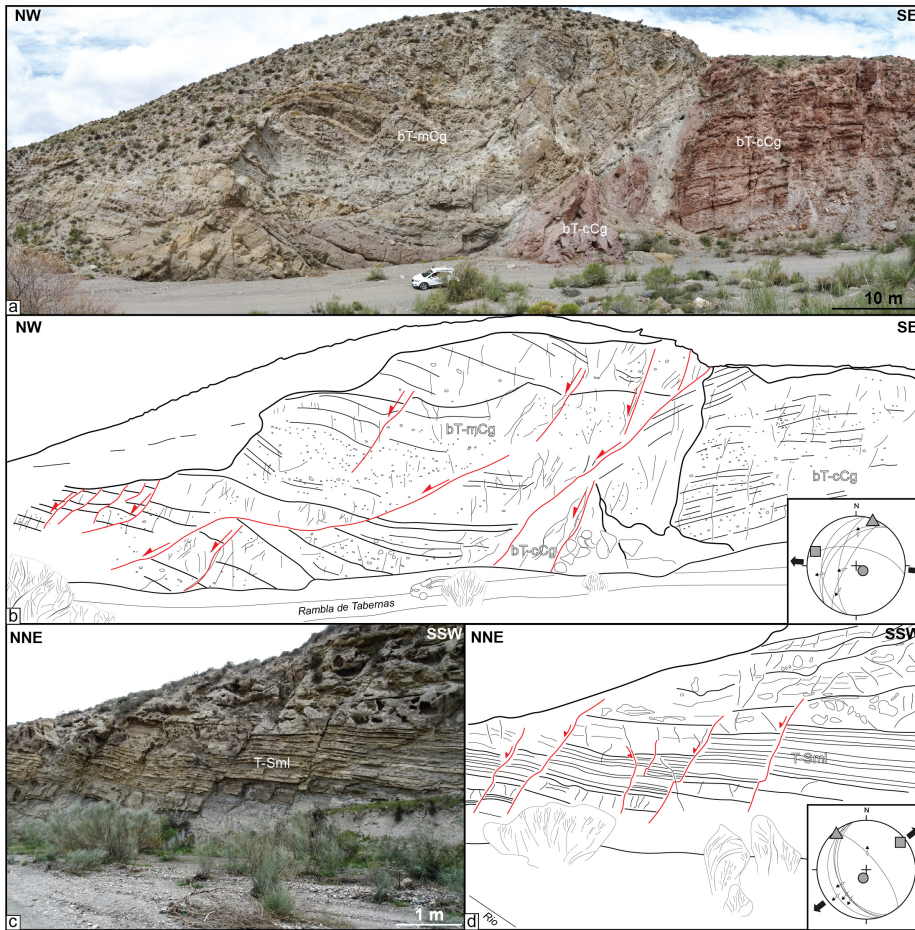
Figure 10 : (a) Drone view taken in the SSW direction of the southern flank of the Sierra de los Filabres at the contact with the Tabernas basin (see Figure 5 for location). Local folding of the micaschist is apparent in the right where the foliation is striking NNE-SSW and is dipping $\sim 25^\circ$ E whereas it is vertical and striking SW-NE in the center of the studied area forming paleosurface. Local cross section highlights the unconformable contact between the Tortonian conglomerates and overlying on the basement. (b) High-resolution drone images of the paleosurface and (c) line-

430 drawing of the foliation revealing secondary folding (see **(d)** stereoplot of fold axes inclined to the NE) and dextral
431 shear zones. Coordinates 37.082777°N/-2.410544°E.
432
433
434



436 **Figure 11** : (a) Field photographs of a NW-SE normal fault at the contact between the Nevado-Filabride micaschists
437 (footwall) and Tortonian sediments (hanging wall). (b) Stratigraphic contact between grey and red basal Tortonian
438 continental conglomerates. These thick Tortonian series rest conformably on the Alpujarride complex (c, d).
439 Coordinates 37.059507°N/-2.478386°E. (e, f) NW-SE normal faults cutting across the NF micaschists basement.
440 These faults that also affect the early Tortonian deposits are sealed by late Tortonian deposits and are therefore syn-
441 depositional. See Figure 5 for location. Al-qz: Alpujarride quartzites; NF-ms: Nevado-Filabride micaschists; bT-cCg:
442 basal Tortonian continental Conglomerates; bT-cSd: basal Tortonian continental Sandstones; T-cSd: Tortonian coarse
443 Sandstones; T-Sd: Tortonian Sandstones; T-Sml: Tortonian Sandstones-marls; C: calcretes. Coordinates
444 37.061279°N/-2.490309°E. Paleostress orientations are in Table S1.
445

446 Both fault slip data and our own observations argue for a regional pre-Tortonian and syn-early Tortonian NNE-SSW
447 directed extension. This direction of extension is also found associated with less well-developed strike-slip regimes
448 (Fig. 8). It is consistent with the D1-D2 phase of brittle deformation found in HOB (Augier et al., 2013). The fact that
449 extension and strike-slip regimes occurred synchronously, or overlap rapidly in time, supports the view that they
450 reflect the same large-scale tectonic setting. The reason why strike-slip faulting is less apparent in the field than
451 expected in models in Fig. 3 is likely to reflect the fact that oblique extension is not fully partitioned between normal
452 and strike-slip components and is actually distributed along oblique structures. Moreover, where strike-slip faults are
453 found they are associated with narrow basins or near the contact between the cover and basement but not in the center
454 of HOB or TB. The NNE-SSW to NW-SE faults appear to postdate the deposition of the early Tortonian red
455 conglomerates and is synchronous with the deposition of marine Tortonian series (Fig. 12). These normal faults
456 currently form half-graben filled with Plio-Quaternary deposits (Guadix, Baza, Alhabia) and are active today. But the
457 importance of extension-related brittle deformation over brittle compression decreases eastwards. Indeed, a late brittle
458 compressional event oriented roughly N-S is described in the literature as a D3 brittle event (e.g. in HOB) associated
459 with reverse and strike-slip faults (Augier et al., 2013). The post-late Tortonian shortening is seen responsible for fold
460 amplification and reverse faulting on the northern limb of Sierra de Alhamilla and Sierra de los Filabres, and locally
461 in the eastern part of the HOB near the termination of left-lateral strike-slip faulting evolution of the Alhama de Murcia
462 fault (Fig. 8).



463
 464 **Figure 12:** (a, b) N-S to NNE-SSW-oriented normal to dextral faults affecting the basal Tortonian continental
 465 conglomerates (bT-cCg) and marine conglomerates (bT-mCg) (Rambla de Tabernas). They form a long and tight E-
 466 W anticlinal crosses the Tabernas basin (see Figure 5 for location). (c, d) Several normal faults observed in Tortonian
 467 sandstones and marls (T-Sml). They are mostly oriented NNW-SSE. Coordinates 37.041648°N/-2.399318°E.
 468 Paleostress orientations are in Table S1.

469 **5. N-S crustal-scale section across the oblique/transform margin of Alboran basin**

470 To examine further the structural relationships between extension and strike-slip faulting across the Alboran margin,
 471 we explore 2D multichannel seismic lines acquired during the MARSIBAL 1-06 cruise (Comas and MARSIBAL1-
 472 06 Scientific Party, 2007) and ESCI cruises (Comas et al., 1995) across the Eastern Alboran basin (EAB). The studied
 473 seismic dataset consists of ~300 km and are deep-penetration multichannel seismic reflection studies (12 s two-way
 474 travel time - TWTT). Here, we study two lines namely MSB08 and MSB07 (see location in Fig. 1). For stratigraphic

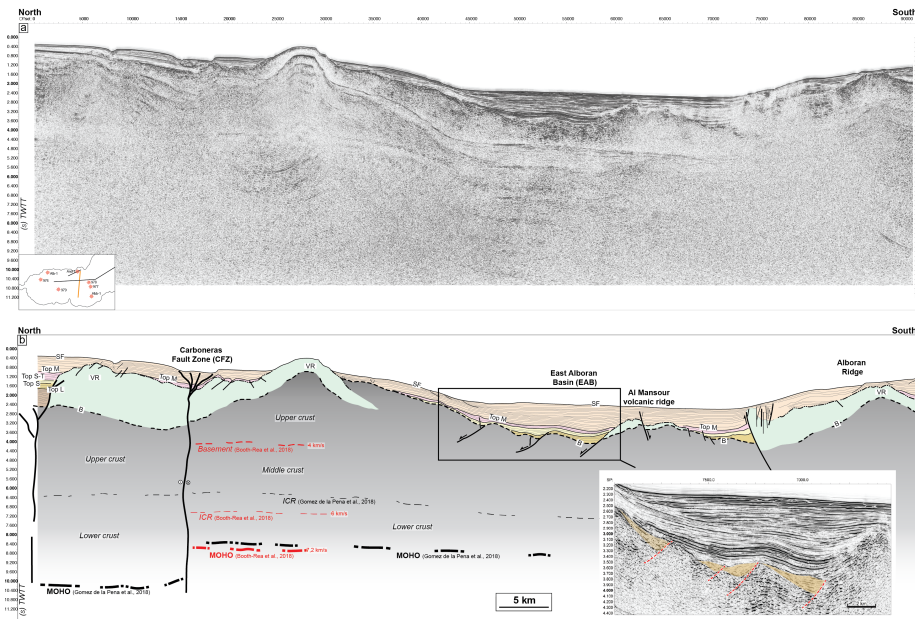
475 and structural correlations between the studied seismic lines, we used the Andaluca-A1 well (Fig. 6a) and results
 476 from ODP 977 and 978 legs (see location in Fig. 1). MSB08 is striking N70°E, slightly oblique to the shoreline. It is
 477 close, and runs parallel, to TM08 line of Gómez de la Peña et al. (2018). It is calibrated by Andaluca-A1 well and
 478 ESCI-Alb1 line (Comas et al., 1995). Line MSB07 stretches in the N-S direction between the EAB in Spain and SAB
 479 to the north of Morocco parallel to line TM09 (Gómez de la Peña et al., 2018) and crosscuts line ESCI Alb2b
 480 presented in Comas et al. (1995) and Booth-Rea et al. (2007) (Fig. 1).

481

482 **5.1 Offshore structures and stratigraphic architecture**

483 The Carboneras Fault is well imaged north of MSB07 (Fig. 13). It forms a negative crustal-scale flower structure
 484 related to left-lateral strike-slip faulting that involves a Moho depth variation between 12 s to 9-8 s TWT after Gómez
 485 de la Peña et al. (2018). It separates a thin continental crust to the North (25-20 km; Fig. 2), from the magmatic calc-
 486 alkaline arc crust of the EAB with a thickness of 18 km in the south (Booth-Rea et al., 2007, 2018; Gómez de la Peña
 487 et al., 2018, 2020a).

488



489

490 **Figure 13** : Seismic reflection line MSB07 (location on Fig. 1). Discontinuous intracrustal reflectors (ICR) imaged
 491 between 3 and 6.5 s TWT, have been interpreted as mylonitic zones within the metamorphic basement (Carbonell et
 492 al., 1998; García-Dueñas et al., 1994; Gómez de la Peña et al., 2018). VR: Volcanic Ridge; B: Acoustic basement;
 493 Top L : Top Langian; Top S: Top Serravallian; Top S-T: top Serravallian-Tortonian; Top M: Top Messinian; SF:
 494 Seafloor.
 495

496

497

498 Reflection seismic data (Figs. 13, 14, 15) collectively show a stratified crust, corresponding to the sediment cover,
499 down to 2.4-4 s TWT, which outlines the acoustic basement with high reflectivity (B). Locally, the top basement
500 reflector coincides with erosional palaeo-relief or high angle normal faults bounding basement highs. These faults are
501 oriented mostly NW-SE to NE-SW and cut across the basement. We recognized on seismic images magmatic additions
502 in the continental crust that are shaped by volcanic edifices exposed on the seafloor (e.g. Chella Bank) or slightly
503 buried (Alboran Ridge) outlined by symmetric downlaps and onlaps of sediments. These constructions form
504 topographic highs such as the Chella Bank on the MSB08 line (Fig. 14), the Alboran Ridge on the MSB07 line (Fig.
505 13) and the Maimonides Ridge on the ESCI-Alb2b line (Fig. 15). All the reflectors corresponding to layers as old as
506 Tortonian are onlapping against the volcanic ridges confirming that the volcanic activity occurred during the middle
507 to late Miocene times, which is shown by Duggen et al. (2008). Some reflectors up to the top Messinian (top M) onlap
508 onto the volcanic ridges probably as a result of Pliocene uplift.

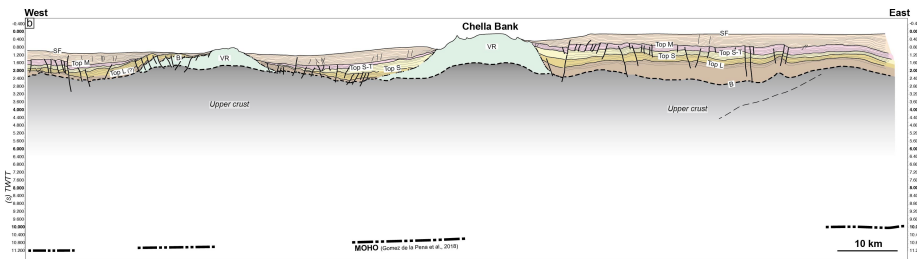
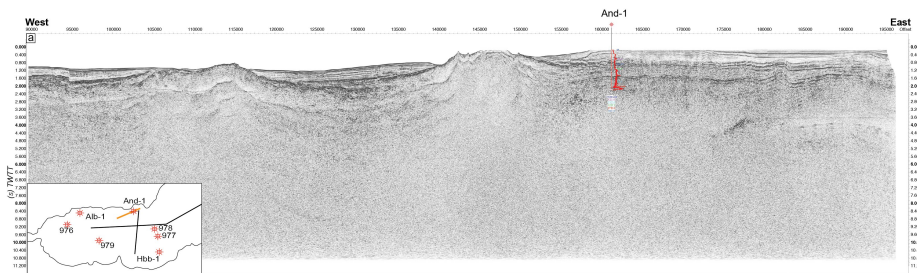
509 The stratigraphy offshore, on the continental crustal domain, is defined by the recognition of five seismic stratigraphic
510 units in Andalucía-A1 well (Jurado and Comas, 1992) labeled I-V from top to base (Figs 6 and 16) and separated by
511 unconformities. The seismostratigraphic units I to V vary in thickness (Fig. 16) and their architecture is conditioned
512 by the occurrence of basement highs and crustal-scale faults.

513 Below the Miocene sedimentary filling, Andalucía-A1 well reveals ~190m of phyllitic and quartzitic meta-sediments
514 (2.4 to 4 s TWT below the Alboran basin, Figs. 13 and 14) topped by Langhian to Tortonian marls (top at ~1.6 to 3.4
515 s TWT below the Alboran basin) interbedded with Tortonian-Messinian tuffs and basaltic lavas. These units have
516 been correlated in the magmatic arc crust of EAB after Gómez de la Peña et al. (2020b). The older deposits (Unit V)
517 Langhian-Serravallian in age, consist of clays and marls with intercalated sands and volcano-clastic deposits. The
518 seismic facies of this Unit V is made of moderate amplitude and low frequency discontinuous reflections packages
519 (Figure 16), and is only present in the Northern Alboran Basin. They are correlated with volcanic series in the EAB
520 (vY3) (Gómez de la Peña et al., 2020b). They pass upward into Serravallian sand-silty clay turbidite (Unit IV) possibly
521 correlated with volcanic series in EAB (vY2 after Gómez de la Peña et al., 2020b). This unit exhibiting low to moderate
522 amplitude, moderate frequency drawing continuous sheeted to disrupted reflectors, is unconformably overlying Unit
523 V and locally onlaps onto the basement. Thickness of Unit IV remains rather thin in the North and East Alboran Basin.
524 It can't be properly identified in the South Balearic Basin, east of the Maimonides volcanic ridge (Fig. 15). The Unit
525 III dated from late Serravallian to late Tortonian is represented by sandstones interbedded with volcano-clastic levels
526 which correlates in EAB with volcanics vY1 unit. Unit III contains internal reflections characterized by low to moderate
527 amplitude, moderate frequency continuous sheeted reflectors. Its thickness remains relatively constant from the NAB
528 to the EAB, and is identified beneath the Messinian Unit II in the South Balearic Basin. Unit II corresponds to the
529 Messinian evaporite, carbonate, volcanic, and volcanoclastic deposits interbedded with fine-grained sediments and is
530 equivalent to unit III of Gómez de la Peña et al. (2020b) in EAB. Seismic facies of Unit II is marked in the Alboran
531 domain by lower amplitudes and lower frequency reflectors. In ESCI-Alb2b line, Unit II increases drastically east of
532 the Maimonides ridge, which delimits the western boundary of the salt deposits in the Western Mediterranean basin

533 during the Messinian Salinity Crisis (Haq et al., 2020). Unit II is topped by Unit I made of Pliocene to Quaternary
 534 clays and sanstones, which are correlated with units II and I in EAB (Gómez de la Peña et al., 2020b). Unit I is marked
 535 by thinly bedded, mostly parallel, high-frequency and low amplitudes reflectors (Fig. 15). Its thickness fluctuates in
 536 response to sedimentary processes (Juan et al., 2016).

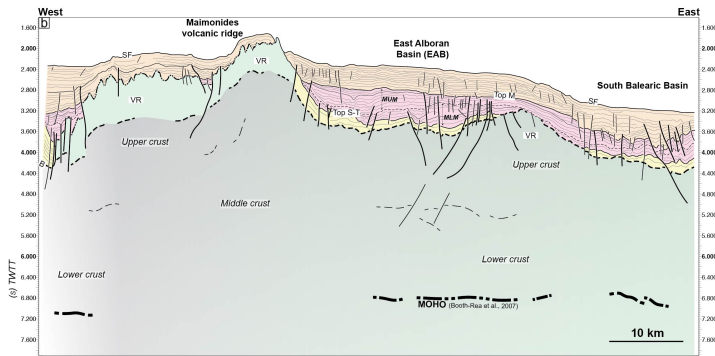
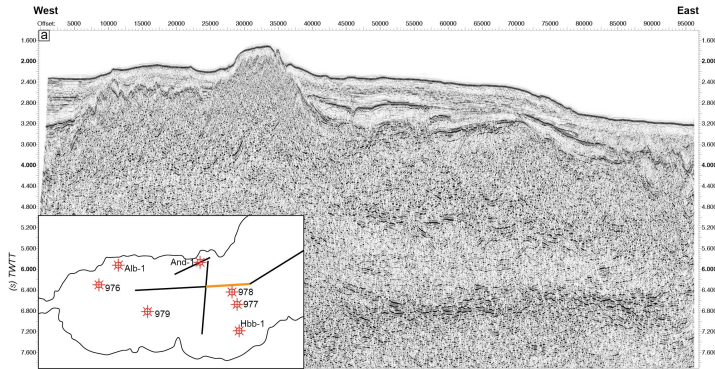
537 Along line MSB08 (Fig. 14) the Langhian-Serravallian (Unit V) is maximum 1600 m-thick (using a P-wave velocity
 538 of 3.2 km/s calculated within Andalucia-A1 well). In EAB, south of Carboneras Fault Zone, the total thickness of Unit
 539 V is only ~300 m on MSB07 (Fig. 13) and is absent in ESCI-Alb2b (Fig. 15). The Serravallian-Tortonian (Unit IV-
 540 III) interval shows only very limited sediment accumulation (~300 m) except near the NW-SE oriented normal faults
 541 where growth geometries are visible. These normal faults are sealed by the Tortonian-Messinian deposits, indicating
 542 a syn-sedimentary faulting during the middle Miocene (Fig. 13). With respect to onshore observations this
 543 sedimentary infill is more continuous and is also much thinner compared to TB and HOB where they are represented
 544 by thick conglomerates and marls/turbidites (> 1km) (Fig. 7), and they are eroded or not deposited along the axes of
 545 the metamorphic domes. The Messinian deposits (Unit II) are ~150-350 m-thick north of CF (MSB07-08 ; Figs. 13,
 546 14) and increase to about 1200 m eastward in the eastern EAB (ESCI-Alb2b ; Fig. 15), and in Algero-Balearic basin
 547 (Gómez de la Peña et al., 2020b). The top Messinian reflector is topped by thick horizontal sedimentary strata, with a
 548 maximum thickness of 1.2 s TWT (~2.4 km assuming a velocity of 2 km/s) on line MSB07, suggesting an important
 549 channel system during the Pliocene.

550 The Pliocene-to-Quaternary series are poorly deformed except in the vicinity of CF and near the Alboran Ridge where
 551 this is associated with south-dipping reverse fault (Fig. 13). This late and still active compressional tectonics is
 552 revealed by the overthrusting of the SAB over the south margin of the EAB (e.g. Martínez-García et al., 2011).
 553

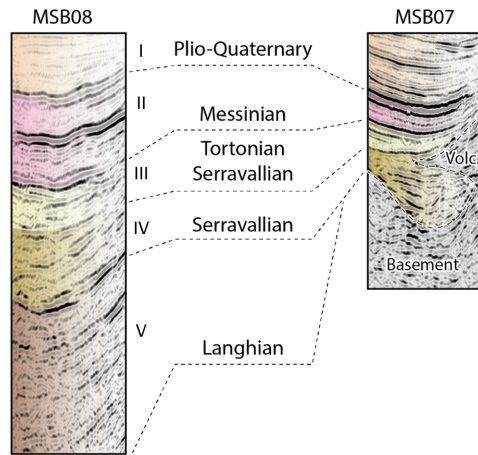


554

555 **Figure 14** : Seismic reflection line MSB08 (see location on **Fig. 1**). See Figure 13 for abbreviations. See also Figure
 556 S3 showing a zoom on the main seismic facies recognized in Andalucia-A1 well.
 557



558 **Figure 15. (a, b)** Seismic reflection line ESCI-Alb2b and interpretation (see Figure 1 for location). Seismic units are
 559 correlated with those defined by Booth-Rea et al. (2007). See Figure 13 for abbreviations.
 560
 561
 562



563
 564 **Figure 16** : Seismic facies of units I to V seen through seismic lines MSB08 close to the shoreline and the line
 565 MSB07, located deeper in the East Alboran Basin.

566 **5.2 N-S crustal cross-section of the Alboran margin accounting for strike-slip faulting**

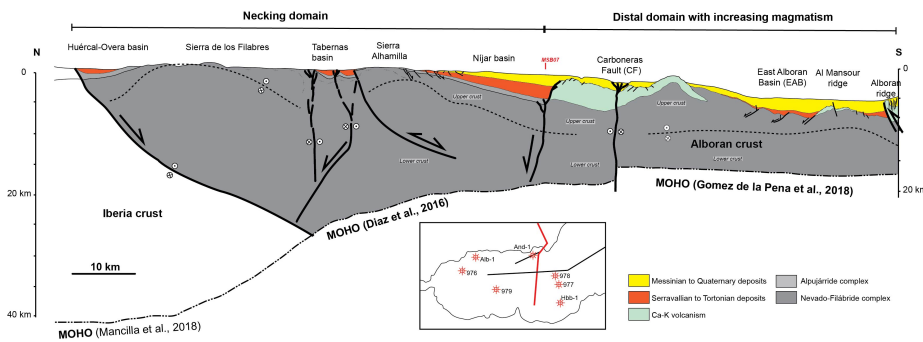
567 Based on subsurface constraints and field data, we present in **Figure 17** a crustal-scale section across the rifted margin,
 568 from the Sierra de las Estancias and Huercal-Overa basin (HOB) to the Alboran ridge that represents the inverted
 569 southern margin of the EAB. The proximal margin, where the crust is 30-35 km-thick, is defined to the North by the
 570 transition between the south Iberia margin, and the metamorphic domain of the Alboran basement exposed in the
 571 Sierra de las Estancias. This continental domain preserves part of the crustal thickness acquired during former Betic
 572 orogenic phase that has been little involved in crustal thinning. The onset of crustal thinning to the south coincides
 573 with the position of the lithospheric tear fault documented by seismology (**Fig. 4**; Mancilla et al., 2015a) and is
 574 recorded by the formation of asymmetric basins of the HOB and TB, shaping the upper neck domain. Orthogonal and
 575 oblique extension in this domain is accommodated by normal and strike-slip faulting during the Tortonian. From the
 576 Sierra de los Filabres to the south, the thickness of the continental crust reduces to 25 km in the Tabernas basin along
 577 the Alpujarras strike-slip fault zone and below the Sierra Alhamilla (**Fig. 17**). The Nijar basin depicts the transition
 578 towards offshore distal domains where the continental crust reaches a thickness of 20 km. The Tortonian and
 579 Messinian marine sediments are also thicker. It is worth noting that a number of volcanic bodies offshore (e.g. Chella
 580 Bank on MSB08) accompany crustal thinning of the continental crust. The Carboneras Fault (CF) brings crusts with
 581 different thicknesses and composition into contact. South of CF, the crustal thickness of the EAB is 18 km and seismic
 582 velocities, especially the occurrence of a high- V_p lower crust, has been considered to indicate the EAB is floored by
 583 a magmatic arc crust (Gómez de la Peña et al., 2018; 2020), formed in a supra-subduction context above the subducting
 584 Alboran slab (Booth-Rea et al., 2018). The crustal thickness of the EAB is compatible with crustal thinning of the
 585 continental margin, and the occurrence of NW-SE-trending faults also recognized onshore despite being slightly older
 586 (Serravallian-Tortonian) suggest that the EAB formed under the same back-arc extension setting, relative to westward

Formatted: Font: Bold

Deleted: (Fig. 17).

588 slab retreat as the whole Alboran margin did. Thus, the magmatic arc crust of the EAB could represent voluminous
 589 magmatic intrusions (e.g. Al Mansour dacite, Alboran Ridge rhyolite dated to ca. 9 Ma; Duggen et al., 2004; Tenderso-
 590 Salmerón et al., 2022; **Fig 17**) formed on the distal rifted margin of Alboran. The investigation of the causes of calc-
 591 alkaline magmatism is beyond the scope of this study, but we suspect it reflects post-subduction arc magmatism
 592 induced by remelting, during extension and delamination, of a metasomatized wedge of mantle lithosphere formed
 593 during a previous subduction event (e.g. Richards, 2009). The fact that calc-alkaline magmatism around 10 Ma that is
 594 10 to 5 myrs after the onset of upper plate extension in the Betic-Alboran region supports this view. Note that in
 595 contrast to Gómez de la Peña et al. (2020) and Booth-Rea et al. (2018) we implicitly assume the magmatic arc crust
 596 of EAB is not a newly formed crust but rather represents a thinned continental crust later intruded by calc-alkaline
 597 magmas. Different crustal domains are expected across a rifted margin that has involved variable amount and types
 598 of mantle-derived magmatism, especially if delamination/subduction occurred during extension. The observation of
 599 contrasting types of crustal domains now juxtaposed in the NS direction is also related to the fact that extension is
 600 oriented perpendicular to the section.

601 Crustal shortening in **Figure 17** is distributed across north-vergent reverse faults below the Alboran Ridge, on the
 602 northern limb of Sierra de Alhamilla, and CF strike-slip fault zone.



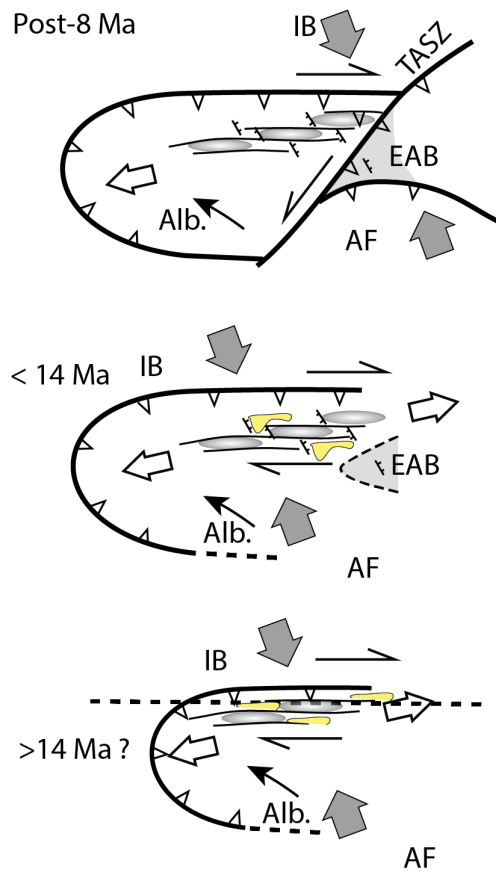
603
 604 **Figure 17.** Crustal-scale cross section of the Alboran margin in the eastern Betics interpreted based on onshore and
 605 offshore constraints presented in the text. Note that in the necking domain the extension of faults downwards to
 606 Moho depths is not imaged on the seismics and therefore largely inspired by inferences from 3D numerical models
 607 (see Fig. 3).
 608
 609

610 **6. Implications**

611 The question of whether the Miocene tectonic evolution of the Betics reflects crustal thinning associated with oblique
612 back-arc rifting as suggested from present-day strain patterns is unclear in the literature. We found based on a
613 comparison between numerical models and basin analyses, fault kinematics and structure of the margin in the eastern
614 Betics compelling evidences that crustal thinning was controlled by oblique extension. Oblique rifting operated since
615 at least the middle Miocene in relation with Alboran slab retreat below the Alboran basin and is kinematically
616 associated with slab tearing and delamination below the central and eastern Betics.

617 One of the most striking tectonic feature of the Alboran margin (**Fig. 17**) is the abrupt N-S crustal thinning oblique to
618 the direction of slab rollback. The history of sediment infill and rates of subsidence in intramontane basins (**Figs. 6**
619 **and 7**) combined with the analyses of fault slip data (**Fig. 8**), and structural data offshore (**Fig. 13**), confirm that brittle
620 extension oriented from N20°E to EW occurred during an interval spanning from the Serravallian-early Tortonian to
621 the late Tortonian (14-8 Ma) (**Fig. 18**). This extension is found associated with both normal and strike-slip regimes.
622 Field tectonic data reveal that N20°E extension is more represented in HOB while the ENE-WSW to EW extension is
623 found related with the evolution of the Almanzora fault zone, Alpujarras fault zone and Tabernas basin flanking the
624 metamorphic domes (**Table S1**). There are additional evidence that EW-directed dextral strike-slip faulting occurred
625 during the Tortonian to the South and West of the HOB. These large-scale transfer fault zones positioned on the slab
626 edge accommodate the differential westward extension that are later cut by Tortonian NW-SE faults. These second
627 set of faults is also observed in the magmatic crust of the EAB offshore but seismic data indicate they are Serravallian-
628 Tortonian in age and therefore older than those identified onshore. We suggest that NW-SE normal faulting could
629 have initiated in the EAB then migrated towards the necking domain as slab retreat progressed and the width of the
630 region affected by crustal thinning widened (**Fig. 18**). Subsidence during the Serravallian-Tortonian appears to have
631 been lower in the EAB compared to intramontane basins onshore. This suggests that the isostatic effect of crustal
632 thinning was compensated by a thermal anomaly in the mantle, heralding the Ca-K magmatism at 11-7 Ma (Duggen
633 et al., 2004, 2008).

634



635

636 **Figure 18:** Tectonic model of the evolution of the northern margin of the Alboran Rift. Large grey and white double
 637 arrows depict shortening, which is parallel to the AF/IB convergence, and the highly oblique extension, respectively.
 638 The thin black arrows show the motion of Alboran relative to Iberia (IB) taken from Figure 4. Half arrows depict
 639 distributed strike-slip faulting in the Betics. NW-SE directed normal fault and strike-slip basins (yellow) are
 640 consistent with the oblique extension. Grey-shaded ellipses represent the metamorphic domes. TASZ : simplified
 641 representation of the Trans-Alboran Shear Zone. We also indicated EAB which mostly formed ca. 9 Ma (Duggen et
 642 al., 2004; Booth-Rea et al., 2018).
 643

644 Several key tectonic features found in the eastern Betics are predicted by 3D models of oblique extension (**Figure 3**).
 645 They include E-W trending normal faults that are prevalent on the upper neck domain (i.e. Sierra de las Estancias and
 646 HOB), and E-W strike-slip faults (Almanzora and Alpujarras fault zones). NW-SE normal faults are associated with

647 more distal domains on the continental margin where crustal thinning is the highest offshore, south of Nijar basin, and
648 in the EAB.

649 Tectonic inversion seems, in contrast, to have been increasingly more important when approaching the Carboneras
650 and Palomares strike-slip faults in the East since the late Tortonian.

651 Ductile thinning associated with the formation of metamorphic domes and exhumation of HP rocks is dated to 23 to
652 16 Ma (Platt et al., 2003; Booth-Rea et al., 2015). This provides time constraint for the beginning of oblique extension
653 and westward slab rollback. Deformation at the future location of the tear fault was probably initially diffuse and
654 resulted in an immature oblique rift system in the South, combined with thrusting in the external zones to the North
655 (**Figure 18**). In the Serravallian (14-13 Ma), accompanying slab steepening, localization of slab tearing, and
656 propagation of thrusting in external zones, oblique extension spread over the whole central Betics. At this time,
657 metamorphic domes exhumed to upper crustal levels (e.g. Vázquez et al., 2011) and recorded the transition from
658 ductile shearing to brittle faulting (**Figure 18**). Brittle E-W-directed stretching and dextral transcurrent deformation
659 formed at this time. The late/post-Tortonian times (from 10-8 Ma) marks a change in the tectonic evolution of the
660 Betics and Alboran domain possibly related to the onset of slab detachment in the eastern Betics (van Hinsbergen et
661 al., 2014; Do Couto et al., 2014; Mancilla et al., 2015a; Martínez-García et al., 2017; d'Acremont et al., 2020; García-
662 Castellanos and Villaseñor, 2011; Spakman et al., 2018). This event is synchronous with the indentation by the
663 magmatic arc crust of the EAB in the Águilas Arc (Ercilla et al., 2022), amplification of the metamorphic domes in
664 the vicinity of the EBSZ (e.g. Alhamilla), transition from Ca-K in EAB to more alkaline magmatism in eastern Betics,
665 and at the regional scale with exhumation in northern Iberia (Rat et al., 2022) and N-S shortening in northern Africa
666 (Jolivet et al., 2021a) (**Figure 18**).

667 In this model, ductile stretching and ductile detachment associated with the development of the domes are the
668 expression of oblique E-W extension. It provides a coherent scheme linking the formation of EW-directed basins in
669 the brittle field associated with strike-slip faulting, and NW-SE/NNW-SSE sedimentary basins (Guadix, Baza,
670 Alhabia) formed in transtension during the Tortonian. As such, the oblique extension is closely associated with STEP
671 faulting required by westward slab rollback. The oblique rifting model we propose explain the formation of the
672 metamorphic domes and intermontane basins and provides insight into crustal deformation, which is broadly
673 consistent with the geodynamic models of slab rollback and tearing since 20 Ma that have been previously proposed
674 for Alboran (Chertova et al., 2014; Spakman et al., 2018). In the latter models, however, the ENE-WSW extension in
675 the central-eastern Betics is related to differential absolute motions between Iberia and the slab decoupled from Iberia
676 by slab tearing. In our scenario, oblique extension is entirely related to westward lateral rollback. It can not be
677 excluded, however, that the effect of mantle-derived slab dragging increased during the late extensional stage, from
678 14-13 Ma, when slab tearing localized.

679 Mid-Miocene high-pressure metamorphism documented in the central Betics (e.g. Platt et al., 2013) was synchronous
680 with slab steepening and subduction that was under way during oblique back-arc extension (**Figure 18**). The case of
681 exhumation of high-pressure rocks in oblique convergence setting associated with near-parallel orogen extension is
682 also documented in other active orogen like Taiwan (Conand et al., 2020).

683 This highly oblique northern Alboran margin differs from typical transform fault margin such as those associated with
684 the Atlantic ocean because it accommodates variations in intra-plate extensional movements, triggered by slab roll-
685 back, not variations in spreading rates. Strike-slip faults may have originated as low-angle normal faults which were
686 later reactivated as thrusts during margin inversion. Similar observations, including metamorphism, strike-slip
687 faulting, high geothermal gradients and volcanism has been made in Seram, north of the Banda Arc, which represents
688 another example of extremely thinned crust formed perpendicular to the direction of the slab rollback (Pownall et al.,
689 2013). Such a narrow rifted margin associated with lithospheric STEP fault defines a class of oblique margin that is
690 expected to be hardly preserved in the geological record due the transient nature of retreating subduction systems.

691
692

693 **Data availability.** This study is based on data compilation. Data used in this study can be found in the appropriate
694 references. Paleostress tensors obtained by the inversion of fault slip data are available online in the Supplement.

695

696 **Supplement.** The supplement related to this article is available on-line at:

697

698 **Competing interests.** The authors declare that they have no conflict of interest.

699 **Authors contribution**

700 ML and FM, conceptualize, prepared figures and tables, compiled and interpreted field structural data and wrote the
701 paper. DC provided and interpreted the seismic lines, reviewed the text and contributed to the writing. AJ carefully
702 examined the implementation of his numerical results and reviewed the text. EM, SC and VM, supervised and
703 coordinate the different project tasks and reviewed the text.

704 **Acknowledgments**

705 Victor Tendero Salmerón, Guillermo Booth-Rea, and an anonymous reviewers are warmly thanked for their comments
706 that greatly improved the manuscript. The stereogram results were obtained using Win-Tensor, a software developed
707 by Dr. Damien Delvaux, Royal Museum for Central Africa, Tervuren, Belgium (Delvaux and Sperner, 2003). The
708 processed seismic data were interpreted using Kingdom IHS Suite© software. This research benefited from
709 discussions and support of OROGEN project, an academic-industry research consortium between TOTAL, CNRS and
710 BRGM.

711

712

713 **References**

- 714 Angrand, P., Mouthereau, F., 2021. Evolution of the Alpine orogenic belts in the Western Mediterranean region as
715 resolved by the kinematics of the Europe-Africa diffuse plate boundary. *Bsgf - Earth Sci Bulletin*.
716 <https://doi.org/10.1051/bsgf/2021031>
- 717 Argus, D.F., Gordon, R.G., DeMets, C., 2011. Geologically current motion of 56 plates relative to the no-net-
718 rotation reference frame. *Geochemistry, Geophysics, Geosystems* 12. <https://doi.org/10.1029/2011gc003751>
- 719 Augier, R., 2004. Evolution tardi-orogénique des Cordillères Bétiques (Espagne) : apports d'une étude intégrée 1
720 vol., [II]-400 p.
- 721 Augier, R., Agard, P., Monié, P., Jolivet, L., Robin, C., Booth-Rea, G., 2005. Exhumation, doming and slab retreat in
722 the Betic Cordillera (SE Spain): in situ ⁴⁰Ar/³⁹Ar ages and P–T–t paths for the Nevado-Filabride complex.
723 *Journal of Metamorphic Geology* 23, 357–381. <https://doi.org/10.1111/j.1525-1314.2005.00581.x>
- 724 Augier, R., Booth-Rea, G., Agard, P., Martínez-Martínez, J.M., Jolivet, L., Azañón, J.M., 2005a. Exhumation
725 constraints for the lower Nevado-Filabride Complex (Betic Cordillera, SE Spain): a Raman thermometry and
726 Tweeku multiequilibrium thermobarometry approach. *Bulletin de la Societe Geologique de France* 176, 403–
727 416. <https://doi.org/10.2113/176.5.403>
- 728 Augier, R., Jolivet, L., Couto, D.D., Negro, F., 2013. From ductile to brittle, late- to post-orogenic evolution of the
729 Betic Cordillera: Structural insights from the northeastern Internal zones. *Bulletin De La Société Géologique De*
730 *France* 184, 405–425. <https://doi.org/10.2113/gssgfbull.184.4-5.405>
- 731 Augier, R., Jolivet, L., Robin, C., 2005b. Late Orogenic doming in the eastern Betic Cordilleras: Final exhumation
732 of the Nevado-Filabride complex and its relation to basin genesis. *Tectonics* 24, n/a-n/a.
733 <https://doi.org/10.1029/2004tc001687>
- 734 Badji, R., Charvis, P., Bracene, R., Galve, A., Badsí, M., Ribodetti, A., Benaissa, Z., Klingelhofer, F., Medaouri,
735 M., Beslier, M.-O., 2014. Geophysical evidence for a transform margin offshore Western Algeria: a witness of a
736 subduction-transform edge propagator? *Geophys J Int* 200, 1029–1045. <https://doi.org/10.1093/gji/ggu454>
- 737 Barcos, L., Balanyá, J.C., Díaz-Azpiroz, M., Expósito, I., Jiménez-Bonilla, A., 2015. Kinematics of the Torcal Shear
738 Zone: Transpressional tectonics in a salient-recess transition at the northern Gibraltar Arc. *Tectonophysics* 663,
739 62–77. <https://doi.org/10.1016/j.tecto.2015.05.002>
- 740 Baudouy, L., Haughton, P.D.W., Walsh, J.J., 2021. Evolution of a Fault-Controlled, Deep-Water Sub-Basin,
741 Tabernas, SE Spain. *Frontiers Earth Sci* 9, 767286. <https://doi.org/10.3389/feart.2021.767286>
- 742 Bessièrre, E., Jolivet, L., Augier, R., Scaillet, S., Précigout, J., Azañón, J.-M., Crespo-Blanc, A., Masini, E., Couto,
743 D.D., 2021. Lateral variations of pressure-temperature evolution in non-cylindrical orogens and 3-D subduction
744 dynamics: the Betic-Rif Cordillera example. *Bsgf - Earth Sci Bulletin*. <https://doi.org/10.1051/bsgf/2021007>
- 745 Bezada, M.J., Humphreys, E.D., Toomey, D.R., Harnafí, M., Dávila, J.M., Gallart, J., 2013. Evidence for slab
746 rollback in westernmost Mediterranean from improved upper mantle imaging. *Earth and Planetary Science*
747 *Letters* 368, 51–60. <https://doi.org/10.1016/j.epsl.2013.02.024>
- 748 Booth-Rea, G., Martínez-Martínez, J.M., Giacomini, F., 2015. Continental subduction, intracrustal shortening, and
749 coeval upper-crustal extension: P-T evolution of subducted south Iberian paleomargin metapelites (Betics, SE
750 Spain). *Tectonophysics* 663, 122–139. <https://doi.org/10.1016/j.tecto.2015.08.036>
- 751 Booth-Rea, G., Ranero, C.R., Grevemeyer, I., 2018. The Alboran volcanic-arc modulated the Messinian faunal
752 exchange and salinity crisis. *Scientific reports* 8, 13015. <https://doi.org/10.1038/s41598-018-31307-7>
- 753 Booth-Rea, G., Ranero, C.R., Martínez-Martínez, J.M., Grevemeyer, I., 2007. Crustal types and Tertiary tectonic
754 evolution of the Alborán sea, western Mediterranean. *Geochemistry, Geophysics, Geosystems* 8, n/a-n/a.
755 <https://doi.org/10.1029/2007gc001639>
- 756 Booth-Rea, G., Azañón, J.-M., Azor, A., García-Dueñas, V., 2004a. Influence of strike-slip fault segmentation on
757 drainage evolution and topography. A case study: the Palomares Fault Zone (southeastern Betics, Spain). *J*
758 *Struct Geol* 26, 1615–1632. <https://doi.org/10.1016/j.jsg.2004.01.007>
- 759 Booth-Rea, G., Azañón, J.M., García-Dueñas, V., 2004b. Extensional tectonics in the northeastern Betics (SE
760 Spain): case study of extension in a multilayered upper crust with contrasting rheologies. *Journal of structural*
761 *geology* 26, 2039–2058. <https://doi.org/10.1016/j.jsg.2004.04.005>
- 762 Borque, M.J., Alzola, A.S., Martín-Rojas, I., Alfaro, P., Molina, S., Cintas, S.R., Caderot, G.R., Lacy, C., Avilés,
763 M., Olmo, A.H., Tortosa, F.J.G., Estévez, A., Gil, A.J., 2019. How Much Nubia-Eurasia Convergence Is
764 Accommodated by the NE End of the Eastern Betic Shear Zone (SE Spain)? Constraints From GPS Velocities.
765 *Tectonics* 38, 271–1839. <https://doi.org/10.1029/2018tc004970>
- 766 Braga, J.C., Martín, J.M., Quesada, C., 2003. Patterns and average rates of late Neogene–Recent uplift of the Betic
767 Cordillera, SE Spain. *Geomorphology* 50, 3–26. [https://doi.org/10.1016/s0169-555x\(02\)00205-2](https://doi.org/10.1016/s0169-555x(02)00205-2)

768 Carbonell, R., Sallares, V., Pous, J., Dañoibeitia, J.J., Queralt, P., Ledo, J.J., Dueñas, V.G., 1998. A multidisciplinary
769 geophysical study in the Betic chain (southern Iberia Peninsula). *Tectonophysics* 288, 137–152.
770 [https://doi.org/10.1016/s0040-1951\(97\)00289-8](https://doi.org/10.1016/s0040-1951(97)00289-8)

771 Clark, S.J.P., Dempster, T.J., 2009. The record of tectonic denudation and erosion in an emerging orogen: an apatite
772 fission-track study of the Sierra Nevada, southern Spain. *Journal of the Geological Society* 166, 87–100.
773 <https://doi.org/10.1144/0016-76492008-041>

774 Comas, M. C., J. J. Dañoibeitia, J. Alvarez-Marón, and J. I. Soto (1995), Crustal reflections and structure in the
775 Alboran Basin. Preliminary results of the ESCI-Alboran survey, *Rev. Soc. Geol. Esp.*, 8(4), 529 – 542.

776 Comas, M.C., García-Dueñas, V., Jurado, M.J., 1992. Neogene tectonic evolution of the Alboran Sea from MCS
777 data. *Geo-mar Lett* 12, 157–164. <https://doi.org/10.1007/bf02084927>

778 Comas, M., and MARSIBAL 1-06 Scientific Party (2007). Preliminary results of Marsibal 1-06 cruise in the
779 Alboran and western Algero-Balearic basins. *Geophys. Res. Abst.*, 9, 10871.

780 Conand, C., Mouthereau, F., Gamme, J., Lin, A.T., Lahfid, A., Daudet, M., Mesalles, L., Giletycz, S., Bonzani, M.,
781 2020. Strain Partitioning and Exhumation in Oblique Taiwan Collision: Role of Rift Architecture and Plate
782 Kinematics. *Tectonics* 39, e2019TC005798. <https://doi.org/10.1029/2019tc005798>

783 Crespo-Blanc, A., Comas, M., Balanyá, J.C., 2016. Clues for a Tortonian reconstruction of the Gibraltar Arc:
784 Structural pattern, deformation diachronism and block rotations. *Tectonophysics* 683, 308–324.
785 <https://doi.org/10.1016/j.tecto.2016.05.045>

786 d’Acremont, E., Lafosse, M., Rabaute, A., Teurquety, G., Couto, D.D., Ercilla, G., Juan, C., Lépinay, B.M.,
787 Lafuerza, S., Galindo-Zaldívar, J., Estrada, F., Vazquez, J.T., Leroy, S., Poort, J., Ammar, A., Gorini, C., 2020.
788 Polyphase Tectonic Evolution of Fore-Arc Basin Related to STEP Fault as Revealed by Seismic Reflection Data
789 From the Alboran Sea (W-Mediterranean). *Tectonics* 39. <https://doi.org/10.1029/2019tc005885>

790 Dalziel, I.W.D., Lawver, L.A., Norton, I.O., Gahagan, L.M., 2013. The Scotia Arc: Genesis, Evolution, Global
791 Significance. *Annu Rev Earth Pl Sc* 41, 767–793. <https://doi.org/10.1146/annurev-earth-050212-124155>

792 Daudet, M., Mouthereau, F., Brichau, S., Crespo-Blanc, A., Gautheron, C., Angrand, P., 2020. Tectono-
793 Stratigraphic and Thermal Evolution of the Western Betic Flysch: Implications for the Geodynamics of South
794 Iberian Margin and Alboran Domain. *Tectonics* 39. <https://doi.org/10.1029/2020tc006093>

795 Dewey, J.F., 1988. Extensional collapse of orogens. *Tectonics* 7, 1123–1139.
796 <https://doi.org/10.1029/tc007i006p01123>

797 Dewey, J.F., Helman, M.L., Knott, S.D., Turco, E., Hutton, D.H.W., 1989. Kinematics of the western
798 Mediterranean. Geological Society, London, Special Publications 45, 265–283.
799 <https://doi.org/10.1144/gsl.sp.1989.045.01.15>

800 Diaz, J., Gallart, J., Carbonell, R., 2016. Moho topography beneath the Iberian-Western Mediterranean region
801 mapped from controlled-source and natural seismicity surveys. *Tectonophysics* 692, 74–85.
802 <https://doi.org/10.1016/j.tecto.2016.08.023>

803 Do Couto, D., Gumiaux, C., Augier, R., Lebreton, N., Folcher, N., Jouannic, G., Jolivet, L., Suc, J., Gorini, C., 2014.
804 Tectonic inversion of an asymmetric graben: Insights from a combined field and gravity survey in the Sorbas
805 basin. *Tectonics* 33, 1360–1385. <https://doi.org/10.1002/2013tc003458>

806 Duggen, S., Hoernle, K., Bogaard, P. van den, Rüpke, L., Morgan, J.P., 2003. Deep roots of the Messinian salinity
807 crisis. *Nature* 422, 602–606. <https://doi.org/10.1038/nature01553>

808 Duggen, S., Hoernle, K., Bogaard, P. van den, Harris, C., 2004. Magmatic evolution of the Alboran region: The role
809 of subduction in forming the western Mediterranean and causing the Messinian Salinity Crisis. *Earth Planet Sc
810 Lett* 218, 91–108. [https://doi.org/10.1016/s0012-821x\(03\)00632-0](https://doi.org/10.1016/s0012-821x(03)00632-0)

811 Duggen, S., Hoernle, K., Klügel, A., Geldmacher, J., Thirlwall, M., Hauff, F., Lowry, D., Oates, N., 2008.
812 Geochemical zonation of the Miocene Alborán Basin volcanism (westernmost Mediterranean): geodynamic
813 implications. *Contrib Mineral Petr* 156, 577. <https://doi.org/10.1007/s00410-008-0302-4>

814 Echeverría, A., Khazaradze, G., Asensio, E., Gárate, J., Dávila, J.M., Suriñach, E., 2013. Crustal deformation in
815 eastern Betics from CuaTeNeo GPS network. *Tectonophysics* 608, 600–612.
816 <https://doi.org/10.1016/j.tecto.2013.08.020>

817 Ercilla, G., Galindo-Zaldívar, J., Estrada, F., Valencia, J., Juan, C., Casas, D., Alonso, B., Comas, M.C., Tendero-
818 Salmerón, V., Casalbore, D., Azpiroz-Zabala, M., Bárcenas, P., Ceramicola, S., Chiocci, F.L., Idárraga-García,
819 J., López-González, N., Mata, P., Palomino, D., Rodríguez-García, J.A., Teixeira, M., Nespereira, J., Vázquez,
820 J.T., Yenes, M., 2022. Understanding the complex geomorphology of a deep sea area affected by continental
821 tectonic indentation: The case of the Gulf of Vera (Western Mediterranean). *Geomorphology* 402, 108126.
822 <https://doi.org/10.1016/j.geomorph.2022.108126>

823 Faccenna, C., Becker, T.W., Auer, L., Billi, A., Boschi, L., Brun, J.P., Capitanio, F.A., Funicello, F., Horváth, F.,
824 Jolivet, L., Piromallo, C., Royden, L., Rossetti, F., Serpelloni, E., 2014. Mantle dynamics in the Mediterranean.
825 *Rev Geophys* 52, 283–332. <https://doi.org/10.1002/2013rg000444>
826 Fortuin, A.R., Krijgsman, W., 2003. The Messinian of the Nijar Basin (SE Spain): sedimentation, depositional
827 environments and paleogeographic evolution. *Sediment Geol* 160, 213–242. [https://doi.org/10.1016/s0037-](https://doi.org/10.1016/s0037-0738(02)00377-9)
828 [0738\(02\)00377-9](https://doi.org/10.1016/s0037-0738(02)00377-9)
829 Fossen, H., Teyssier, C., Whitney, D.L., 2013. Transtensional folding. *Journal of structural geology* 56, 89–102.
830 <https://doi.org/http://dx.doi.org/10.1016/j.jsg.2013.09.004>
831 Fossen, H., Tikoff, B., 1998. Extended models of transpression and transtension, and application to tectonic settings.
832 Geological Society, London, Special Publications 135, 15–33. <https://doi.org/10.1144/gsl.sp.1998.135.01.02>
833 Galindo-Zaldivar, J., Gonzalez-Lodeiro, F., Jabaloy, A., 2015. Progressive extensional shear structures in a
834 detachment contact in the Western Sierra Nevada (Betic Cordilleras, Spain). *Geodin Acta* 3, 73–85.
835 <https://doi.org/10.1080/09853111.1989.11105175>
836 Galindo-Zaldivar, J., Gil, A.J., Borque, M.J., González-Lodeiro, F., Jabaloy, A., Marin-Lechado, C., Ruano, P.,
837 Galdeano, C.S. de, 2003. Active faulting in the internal zones of the central Betic Cordilleras (SE, Spain). *J*
838 *Geodyn* 36, 239–250. [https://doi.org/10.1016/s0264-3707\(03\)00049-8](https://doi.org/10.1016/s0264-3707(03)00049-8)
839 Gallais, F., Graindorge, D., Gutscher, M.-A., Klaeschen, D., 2013. Propagation of a lithospheric tear fault (STEP)
840 through the western boundary of the Calabrian accretionary wedge offshore eastern Sicily (Southern Italy).
841 *Tectonophysics* 602, 141–152. <https://doi.org/10.1016/j.tecto.2012.12.026>
842 García-Castellanos, D., Villaseñor, A., 2012. Messinian salinity crisis regulated by competing tectonics and erosion
843 at the Gibraltar arc. *Nature* 480, 359–363. <https://doi.org/10.1038/nature10651>
844 García-Dueñas, V., Banda, E., Torné, M., Córdoba, D., Group, E.-B.W., 1994. A deep seismic reflection survey
845 across the Betic Chain (southern Spain): first results. *Tectonophysics* 232, 77–89. [https://doi.org/10.1016/0040-](https://doi.org/10.1016/0040-1951(94)90077-9)
846 [1951\(94\)90077-9](https://doi.org/10.1016/0040-1951(94)90077-9)
847 Giaconia, F., Booth-Rea, G., Martínez-Martínez, J.M., Azañón, J.M., Pérez-Peña, J.V., Pérez-Romero, J., Villegas,
848 I., 2012. Geomorphic evidence of active tectonics in the Sierra Alhamilla (eastern Betics, SE Spain).
849 *Geomorphology* 145, 90–106. <https://doi.org/10.1016/j.geomorph.2011.12.043>
850 Giaconia, F., Booth-Rea, G., Martínez-Martínez, J.M., Azañón, J.M., Pérez-Romero, J., Villegas, I., 2013. Mountain
851 front migration and drainage captures related to fault segment linkage and growth: The Polopos transpressive
852 fault zone (southeastern Betics, SE Spain). *J Struct Geol* 46, 76–91. <https://doi.org/10.1016/j.jsg.2012.10.005>
853 Giaconia, F., Booth-Rea, G., Martínez-Martínez, J.M., Azañón, J.M., Storti, F., Artioni, A., 2014. Heterogeneous
854 extension and the role of transfer faults in the development of the southeastern Betic basins (SE Spain).
855 *Tectonics* 33, 2467–2489. <https://doi.org/10.1002/2014tc003681>
856 Giaconia, F., Booth-Rea, G., Ranero, C.R., Gràcia, E., Bartolome, R., Calahorra, A., Iacono, C.L., Vendrell,
857 M.G., Cameselle, A.L., Costa, S., Peña, L.G. de la, Martínez-Loriente, S., Perea, H., Viñas, M., 2015.
858 Compressional tectonic inversion of the Algero-Balearic basin: Latest Miocene to present oblique
859 convergence at the Palomares margin (Western Mediterranean): Tectonic Inversion of Palomares Margin.
860 *Tectonics* 34, 1516–1543. <https://doi.org/10.1002/2015tc003861>
861 Gomez-Pugnaire, M.T., Fernandez-Soler, J.M., 1987. High-pressure metamorphism in metabasites from the Betic
862 Cordilleras (S.E. Spain) and its evolution during the Alpine orogeny. *Contrib Mineral Petr* 95, 231–244.
863 <https://doi.org/10.1007/bf00381273>
864 Gómez de la Peña, L.G. de la, Grevemeyer, I., Kopp, H., Díaz, J., Gallart, J., Booth-Rea, G., Gràcia, E., Ranero,
865 C.R., 2020a. The Lithospheric Structure of the Gibraltar Arc System From Wide-Angle Seismic Data. *J Geophys*
866 *Res Solid Earth* 125. <https://doi.org/10.1029/2020jb019854>
867 Gómez de la Peña, L.G. de la, Ranero, C.R., Gràcia, E., 2018. The Crustal Domains of the Alboran Basin (Western
868 Mediterranean). *Tectonics* 37, 3352–3377. <https://doi.org/10.1029/2017tc004946>
869 Gómez de la Peña, L.G. de la, Ranero, C.R., Gràcia, E., Booth-Rea, G., 2020b. The evolution of the westernmost
870 Mediterranean basins. *Earth-sci Rev* 103445. <https://doi.org/10.1016/j.earscirev.2020.103445>
871 Govers, R., Wortel, M.J.R., 2005. Lithosphere tearing at STEP faults: response to edges of subduction zones. *Earth*
872 *Planet Sc Lett* 236, 505–523. <https://doi.org/10.1016/j.epsl.2005.03.022>
873 Haq, B., Gorini, C., Baur, J., Moneron, J., & Rubino, J.-L. (2020). Deep Mediterranean's Messinian evaporite giant:
874 How much salt? *Global and Planetary Change*, 184, 103052.
875 [doi:https://doi.org/10.1016/j.gloplacha.2019.103052](https://doi.org/10.1016/j.gloplacha.2019.103052)
876 Houghton, P.D.W., 2000. Evolving turbidite systems on a deforming basin floor, Tabernas, SE Spain.
877 *Sedimentology* 47, 497–518. <https://doi.org/10.1046/j.1365-3091.2000.00293.x>

878 Haughton, P.D.W., 1994. Deposits of deflected and ponded turbidity currents, Sorbas Basin, Southeast Spain. *J*
879 *Sediment Res* 64, 233–246. <https://doi.org/10.1306/d4267d6b-2b26-11d7-8648000102c1865d>
880 Heit, B., Mancilla, F. de L., Yuan, X., Morales, J., Stich, D., Martín, R., Molina-Aguilera, A., 2017. Tearing of the
881 mantle lithosphere along the intermediate-depth seismicity zone beneath the Gibraltar Arc: The onset of
882 lithospheric delamination. *Geophys Res Lett* 44, 4027–4035. <https://doi.org/10.1002/2017gl073358>
883 Hodgson, D.M., Haughton, P.D.W., 2004. Impact of syndepositional faulting on gravity current behaviour and deep-
884 water stratigraphy: Tabernas-Sorbas Basin, SE Spain. *Geological Soc Lond Special Publ* 222, 135–158.
885 <https://doi.org/10.1144/gsl.sp.2004.222.01.08>
886 Jabaloy-Sánchez, A., Talavera, C., Rodríguez-Peces, M.J., Vázquez-Vílchez, M., Evans, N.J., 2021. U-Pb
887 geochronology of detrital and igneous zircon grains from the Águilas Arc in the Internal Betics (SE Spain):
888 Implications for Carboniferous-Permian paleogeography of Pangea. *Gondwana Res* 90, 135–158.
889 <https://doi.org/10.1016/j.gr.2020.10.013>
890 Janowski, M., Loget, N., Gautheron, C., Barbarand, J., Bellahsen, N., Driessche, J.V. den, Babault, J., Meyer, B.,
891 2017. Neogene exhumation and relief evolution in the eastern Betics (SE Spain): Insights from the Sierra de
892 Gador. *Terra Nova* 29, 91–97. <https://doi.org/10.1111/ter.12252>
893 Johnson, C., Harbury, N., Hurford, A.J., 1997. The role of extension in the Miocene denudation of the Nevado-
894 Filábride Complex, Betic Cordillera (SE Spain). *Tectonics* 16, 189–204. <https://doi.org/10.1029/96tc03289>
895 Jolivet, L., Baudin, T., Calassou, S., Chevrot, S., Ford, M., Issautier, B., Lasseur, E., Masini, E., Manatschal, G.,
896 Mouthereau, F., Thion, I., Vidal, O., 2021a. Geodynamic evolution of a wide plate boundary in the Western
897 Mediterranean, near-field versus far-field interactions. *Bsgf - Earth Sci Bulletin* 192, 48.
898 <https://doi.org/10.1051/bsgf/2021043>
899 Jolivet, L., Faccenna, C., 2000. Mediterranean extension and the Africa-Eurasia collision. *Tectonics* 19, 1095–1106.
900 <https://doi.org/10.1029/2000tc900018>
901 Jolivet, L., Menant, A., Roche, V., Le Pourhiet, L., Maillard, A., Augier, R., Couto, D.D., Gorini, C., Thion, I.,
902 Canva, A., 2021b. Transfer zones in Mediterranean back-arc regions and tear faults. *Bsgf - Earth Sci Bulletin*
903 192, 11. <https://doi.org/10.1051/bsgf/2021006>
904 Jourdon, A., Kergaravat, C., Duclaux, G., Huguen, C., 2021. Looking beyond kinematics: 3D thermo-mechanical
905 modelling reveals the dynamics of transform margins. *Solid Earth* 12, 1211–1232. [https://doi.org/10.5194/se-12-](https://doi.org/10.5194/se-12-1211-2021)
906 [1211-2021](https://doi.org/10.5194/se-12-1211-2021)
907 Juan, C., Ercilla, G., Javier Hernández-Molina, F., Estrada, F., Alonso, B., Casas, D., . . . Ammar, A. (2016).
908 Seismic evidence of current-controlled sedimentation in the Alboran Sea during the Pliocene and Quaternary:
909 Palaeoceanographic implications. *Marine Geology*, 378, 292-311.
910 doi:<https://doi.org/10.1016/j.margeo.2016.01.006>
911 Jurado, M.J., Comas, M.C., 1992. Well log interpretation and seismic character of the cenozoic sequence in the
912 northern Alboran Sea. *Geo-Marine Letters* 12, 129–136.
913 Kleverlaan, K., 1989. Neogene history of the Tabernas basin (SE Spain) and its Tortonian submarine fan
914 development. *Geologie en Mijnbouw* 421–432.
915 Kleverlaan, K., 1989. Three distinctive feeder-lobe systems within one time slice of the Tortonian Tabernas fan, SE
916 Spain. *Sedimentology* 36, 25–45. <https://doi.org/10.1111/j.1365-3091.1989.tb00818.x>
917 Kleverlaan, K., 1987. Gordo megabed: a possible seismite in a tortonian submarine fan, tabernas basin, province
918 almeria, southeast spain. *Sediment Geol* 51, 165–180. [https://doi.org/10.1016/0037-0738\(87\)90047-9](https://doi.org/10.1016/0037-0738(87)90047-9)
919 Koulali, A., Ouazar, D., Tahayt, A., King, R.W., Vernant, P., Reilinger, R.E., McClusky, S., Mourabit, T., Davila,
920 J.M., Amraoui, N., 2011. New GPS constraints on active deformation along the Africa–Iberia plate boundary.
921 *Earth Planet Sc Lett* 308, 211–217. <https://doi.org/10.1016/j.epsl.2011.05.048>
922 Larouzière, F.D.D., Bolze, J., Bordet, P., Hernandez, J., Montenat, C., d'Estevou, P.O., 1988. The Betic segment of
923 the lithospheric Trans-Alboran shear zone during the Late Miocene. *Tectonophysics* 152, 41–52.
924 [https://doi.org/10.1016/0040-1951\(88\)90028-5](https://doi.org/10.1016/0040-1951(88)90028-5)
925 Le Pourhiet, J., Huet, B., May, D.A., Labrousse, L., Jolivet, L., 2012. Kinematic interpretation of the 3D shapes of
926 metamorphic core complexes: 3D SHAPES OF MCCs. *Geochem Geophys Geosystems* 13,
927 <https://doi.org/10.1029/2012gc004271>
928 Lonergan, L., White, N., 1997. Origin of the Betic-Rif mountain belt. *Tectonics* 16, 504–522.
929 <https://doi.org/10.1029/96tc03937>
930 Mancilla, F. de L., Booth-Rea, G., Stich, D., Pérez-Peña, J.V., Morales, J., Azañón, J.M., Martín, R., Giaconia, F.,
931 2015a. Slab rupture and delamination under the Betics and Rif constrained from receiver functions.
932 *Tectonophysics*. <https://doi.org/10.1016/j.tecto.2015.06.028>

Deleted: Hinsbergen, D.J.J., Vissers, R.L.M., Spakman, W., 2014. Origin and consequences of western Mediterranean subduction, rollback, and slab segmentation. *Tectonics* 33, 393–419. <https://doi.org/10.1002/2013tc003349>

Deleted: L

Deleted: [https://doi.org/10.1016/0040-1951\(88\)90028-5](https://doi.org/10.1016/0040-1951(88)90028-5)

Moved (insertion) [3]

939 Mancilla, F. de L., Heit, B., Morales, J., Yuan, X., Stich, D., Molina-Aguilera, A., Azañón, J.M., Martín, R., 2018.
940 A STEP fault in Central Betics, associated with lateral lithospheric tearing at the northern edge of the Gibraltar
941 arc subduction system. *Earth Planet Sc Lett* 486, 32–40. <https://doi.org/10.1016/j.epsl.2018.01.008>
942 Mancilla, F. de L., Stich, D., Morales, J., Martín, R., Díaz, J., Pazos, A., Córdoba, D., Pulgar, J.A., Ibarra, P.,
943 Harnafi, M., Gonzalez-Lodeiro, F., 2015b. Crustal thickness and images of the lithospheric discontinuities in the
944 Gibraltar arc and surrounding areas. *Geophysical Journal International* 203, 1804–1820.
945 <https://doi.org/10.1093/gji/ggv390>
946 Martín, J.M., Braga, J.C., Rivas, P., 1989. Coral successions in Upper Tortonian reefs in SE Spain. *Lethaia* 22, 271–
947 286. <https://doi.org/10.1111/j.1502-3931.1989.tb01342.x>
948 Martín, J.M., Braga, J.C., 1994. Messinian events in the Sorbas Basin in southeastern Spain and their implications in
949 the recent history of the Mediterranean. *Sediment Geol* 90, 257–268. [https://doi.org/10.1016/0037-](https://doi.org/10.1016/0037-0738(94)90042-6)
950 [0738\(94\)90042-6](https://doi.org/10.1016/0037-0738(94)90042-6)
951 Martínez-García, P., Comas, M., Lonergan, L., Watts, A.B., 2017. From Extension to Shortening: Tectonic
952 Inversion Distributed in Time and Space in the Alboran Sea, Western Mediterranean. *Tectonics* 36, 2777–2805.
953 <https://doi.org/10.1002/2017tc004489>
954 Martínez-García, P., Soto, J.I., Comas, M., 2011. Recent structures in the Alboran Ridge and Yusuf fault zones
955 based on swath bathymetry and sub-bottom profiling: evidence of active tectonics. *Geo-mar Lett* 31, 19–36.
956 <https://doi.org/10.1007/s00367-010-0212-0>
957 Martínez-Martínez, J.M., Azañón, J.M., 1997. Mode of extensional tectonics in the southeastern Betics (SE Spain):
958 Implications for the tectonic evolution of the peri-Alborán orogenic system. *Tectonics* 16, 205–225.
959 <https://doi.org/10.1029/97tc00157>
960 Martínez-Martínez, J.M., Booth-Rea, G., Azañón, J.M., Torcal, F., 2006. Active transfer fault zone linking a
961 segmented extensional system (Betics, southern Spain): Insight into heterogeneous extension driven by edge
962 delamination. *Tectonophysics* 422, 159–173. <https://doi.org/10.1016/j.tecto.2006.06.001>
963 Martínez-Martínez, J.M., Soto, J.I., Balanyá, J.C., 2002. Orthogonal folding of extensional detachments: Structure
964 and origin of the Sierra Nevada elongated dome (Betics, SE Spain). *Tectonics* 21, 3-1-3–20.
965 <https://doi.org/10.1029/2001tc001283>
966 Martínez-Martínez, J.M., Soto, J.I., Balanyá, J.C., 2004. Elongated domes in extended orogens: A mode of mountain
967 uplift in the Betics (southeast Spain), in: *Special Paper 380: Gneiss Domes in Orogeny*. Geological Society of
968 America, pp. 243–265. <https://doi.org/10.1130/0-8137-2380-9.243>
969 Martínez-Martos, M., Galindo-Zaldívar, J., Martínez-Moreno, F.J., Calvo-Rayó, R., Galdeano, C.S. de, 2017.
970 Superposition of tectonic structures leading elongated intramontane basin: the Alhabia basin (Internal Zones,
971 Betic Cordillera). *Int J Earth Sci* 106, 2461–2471. <https://doi.org/10.1007/s00531-016-1442-9>
972 Meighan, H.E., Brink, U. ten, Pulliam, J., 2013. Slab tears and intermediate-depth seismicity: slab tears and
973 intermediate seismicity. *Geophys Res Lett* 40, 4244–4248. <https://doi.org/10.1002/grl.50830>
974 Meijninger, B.M.L., Vissers, R.L.M., 2006. Miocene extensional basin development in the Betic Cordillera, SE
975 Spain revealed through analysis of the Alhama de Murcia and Crevillente Faults: Miocene extensional basin
976 development in the Betic Cordillera. *Basin Res* 18, 547–571. <https://doi.org/10.1111/j.1365-2117.2006.00308.x>
977 Montecat, C., D'Estevou, P.O., 1992. Geodynamics of the Eastern Betic late Neogene Basins. A Review. *Física de*
978 *la Tierra* 57–75.
979 Montecat, C., d'Estevou, P.O., 1999. The diversity of late Neogene sedimentary basins generated by wrench faulting
980 in the eastern Betic Cordillera, SE Spain. *J Petrol Geol* 22, 61–80. [https://doi.org/10.1111/j.1747-](https://doi.org/10.1111/j.1747-5457.1999.tb00459.x)
981 [5457.1999.tb00459.x](https://doi.org/10.1111/j.1747-5457.1999.tb00459.x)
982 Mora, M., 1993. Tectonic and sedimentary analysis of the Huercal-Overa region, South East Spain, Betic Cordillera.
983 University of Oxford, 300 pp.
984 Moragues, L., Ruano, P., Azañón, J.M., Garrido, C.J., Hidas, K., Booth-Rea, G., 2021. Two Cenozoic Extensional
985 Phases in Mallorca and Their Bearing on the Geodynamic Evolution of the Western Mediterranean. *Tectonics*
986 40. <https://doi.org/10.1029/2021tc006868>.
987 Mouthereau, F., Angrand, P., Jourdon, A., Ternois, S., Fillon, C., Calassou, S., Chevrot, S., Ford, M., Jolivet, L.,
988 Manatschal, G., Masini, E., Thion, I., Vidal, O., Baudin, T., 2021. Cenozoic mountain building and topographic
989 evolution in Western Europe: impact of billions of years of lithosphere evolution and plate kinematics. *Bsgf -*
990 *Earth Sci Bulletin* 192, 56. <https://doi.org/10.1051/bsgf/2021040>
991 Mouthereau, F., Filleaudeau, P., Vacherat, A., Pik, R., Lacombe, O., Fellin, M.G., Castellort, S., Christophoul, F.,
992 Masini, E., 2014. Placing limits to shortening evolution in the Pyrenees: Role of margin architecture and
993 implications for the Iberia/Europe convergence. *Tectonics* 33, 2283–2314. <https://doi.org/10.1002/2014tc003663>

Formatted: English (US)

994 Neuharth, D., Brune, S., Glerum, A., Morley, C.K., Yuan, X., Braun, J., 2021. Flexural strike-slip basins. *Geology*.
995 <https://doi.org/10.1130/g49351.1>

996 Nocquet, J.-M., 2012. Present-day kinematics of the Mediterranean: A comprehensive overview of GPS results.
997 *Tectonophysics* 579, 220–242. <https://doi.org/10.1016/j.tecto.2012.03.037>

998 Okay, A.I., Tüysüz, O., Kaya, Ş., 2004. From transpression to transtension: changes in morphology and structure
999 around a bend on the North Anatolian Fault in the Marmara region. *Tectonophysics* 391, 259–282.
1000 <https://doi.org/10.1016/j.tecto.2004.07.016>

1001 Palano, M., González, P.J., Fernández, J., 2015. The Diffuse Plate boundary of Nubia and Iberia in the Western
1002 Mediterranean: Crustal deformation evidence for viscous coupling and fragmented lithosphere. *Earth and
1003 Planetary Science Letters* 430, 439–447. <https://doi.org/10.1016/j.epsl.2015.08.040>

1004 Palano, M., González, P.J., Fernández, J., 2013. Strain and stress fields along the Gibraltar Orogenic Arc:
1005 Constraints on active geodynamics. *Gondwana Res* 23, 1071–1088. <https://doi.org/10.1016/j.gr.2012.05.021>

1006 Palomeras, I., Thurner, S., Levander, A., Liu, K., Villaseñor, A., Carbonell, R., Harnafi, M., 2014. Finite-frequency
1007 Rayleigh wave tomography of the western Mediterranean: Mapping its lithospheric structure. *Geochemistry,
1008 Geophysics, Geosystems* 15, 140–160. <https://doi.org/10.1002/2013gc004861>

1009 Pedrera, A., Galindo-Zaldívar, J., Galdeano, C.S. de, López-Garrido, A.C., 2007. Fold and fault interactions during
1010 the development of an elongated narrow basin: The Almanzora Neogene-Quaternary Corridor (SE Betic
1011 Cordillera, Spain): FOLD AND FAULT INTERACTIONS. *Tectonics* 26, n/a-n/a.
1012 <https://doi.org/10.1029/2007tc002138>

1013 Pedrera, A., Galindo-Zaldívar, J., Ruíz-Constán, A., Duque, C., Marín-Lechado, C., Serrano, I., 2009. Recent large
1014 fold nucleation in the upper crust: Insight from gravity, magnetic, magnetotelluric and seismicity data (Sierra de
1015 Los Filabres–Sierra de Las Estancias, Internal Zones, Betic Cordillera). *Tectonophysics* 463, 145–160.
1016 <https://doi.org/10.1016/j.tecto.2008.09.037>

1017 Pedrera, A., Galindo-Zaldívar, J., Tello, A., Marín-Lechado, C., 2010. Intramontane basin development related to
1018 contractional and extensional structure interaction at the termination of a major sinistral fault: The Huércal-
1019 Overa Basin (Eastern Betic Cordillera). *J Geodyn* 49, 271–286. <https://doi.org/10.1016/j.jog.2010.01.008>

1020 Pickering, K.T., Hodgson, D.M., Platzman, E., Clark, J.D., Stephens, C., 2001. A New Type of Bedform Produced
1021 by Backfilling Processes in a Submarine Channel, Late Miocene, Tabernas-Sorbas Basin, SE Spain. *J Sediment
1022 Res* 71, 692–704. <https://doi.org/10.1306/2dc40960-0e47-11d7-8643000102c1865d>

1023 Pindell, J.L., Kennan, L., 2009. Tectonic evolution of the Gulf of Mexico, Caribbean and northern South America in
1024 the mantle reference frame: an update. *Geological Soc Lond Special Publ* 328, 1–55.
1025 <https://doi.org/10.1144/sp328.1>

1026 Platt, J.P., Behr, W.M., Johannesen, K., Williams, J.R., 2013. The Betic-Rif Arc and Its Orogenic Hinterland: A
1027 Review. *Annual Review of Earth and Planetary Sciences* 41, 313–357. <https://doi.org/10.1146/annurev-earth-050212-123951>

1028 Platt, J.P., Kelley, S.P., Carter, A., Orozco, M., 2005. Timing of tectonic events in the Alpujarride Complex, Betic
1029 Cordillera, southern Spain. *J Geol Soc London* 162, 451–462. <https://doi.org/10.1144/0016-764903-039>

1030 Platt, J.P., Whitehouse, M.J., Kelley, S.P., Carter, A., Hollick, L., 2003. Simultaneous extensional exhumation
1031 across the Alboran Basin: Implications for the causes of late orogenic extension. *Geology* 31, 251–254.
1032 [https://doi.org/10.1130/0091-7613\(2003\)031<0251:seeata>2.0.co;2](https://doi.org/10.1130/0091-7613(2003)031<0251:seeata>2.0.co;2)

1033 Platt, J.P., Anczkiewicz, R., Soto, J.-I., Kelley, S.P., Thirlwall, M., 2006. Early Miocene continental subduction and
1034 rapid exhumation in the western Mediterranean. *Geology* 34, 981–984. <https://doi.org/10.1130/g22801a.1>

1035 Platt, J.P., Vissers, R.L.M., 1989. Extensional collapse of thickened continental lithosphere: A working hypothesis
1036 for the Alboran Sea and Gibraltar arc. *Geology* 17, 540–543. [https://doi.org/10.1130/0091-7613\(1989\)017<0540:ecotcl>2.3.co;2](https://doi.org/10.1130/0091-7613(1989)017<0540:ecotcl>2.3.co;2)

1037 Platt, J.P., Whitehouse, M.J., 1999. Early Miocene high-temperature metamorphism and rapid exhumation in the
1038 Betic Cordillera (Spain): evidence from U–Pb zircon ages. *Earth and Planetary Science Letters* 171, 591–605.

1039 Plattzman, E.S., 1992. Paleomagnetic rotations and the kinematics of the Gibraltar arc. *Geology* 20, 311–314.
1040 [https://doi.org/10.1130/0091-7613\(1992\)020<0311:pratko>2.3.co;2](https://doi.org/10.1130/0091-7613(1992)020<0311:pratko>2.3.co;2)

1041 Poisson, A., Guezou, J.C., Ozturk, A., Inan, S., Temiz, H., Gürsöy, H., Kavak, K.S., ÖZDEN, S., 1996. Tectonic
1042 Setting and Evolution of the Sivas Basin, Central Anatolia, Turkey. *International Geology Review* 38, 838–853.
1043 <https://doi.org/10.1080/00206819709465366>

1044 Poisson, A.M., Morel, J.L., Andrieux, J., Coulon, M., Wernli, R., Guernet, C., 1999. The origin and development of
1045 neogene basins in the SE Betic Cordillera (SE Spain): a case study of the Tabernas-Sorbas and Huercal Overa
1046 basins. *J Petrol Geol* 22, 97–114. <https://doi.org/10.1111/j.1747-5457.1999.tb00461.x>

1049 Pownall, J.M., Hall, R., Watkinson, I.M., 2013. Extreme extension across Seram and Ambon, eastern Indonesia:
1050 evidence for Banda slab rollback. *Solid Earth* 4, 277–314. <https://doi.org/10.5194/se-4-277-2013>

1051 Rat, J., Mouthereau, F., Bricchau, S., Crémades, A., Bernet, M., Balvay, M., Ganne, J., Lahfid, A., Gautheron, C.,
1052 2019. Tectonothermal Evolution of the Cameros Basin: Implications for Tectonics of North Iberia. *Tectonics* 38,
1053 440–469. <https://doi.org/10.1029/2018tc005294>

1054 Rat, J., Mouthereau, F., Bricchau, S., Vacherat, A., Fillon, C., Gautheron, C., 2022. Timing and distribution of
1055 exhumation in the Ebro basin reveal a plate-scale 10 Ma geodynamic event. *Global Planet Change* 103973.
1056 <https://doi.org/10.1016/j.gloplacha.2022.103973>

1057 Reichert, K., Hübscher, C., 2006. Evidence for a seafloor rupture of the Carboneras Fault Zone (southern Spain):
1058 Relation to the 1522 Almería earthquake? *J Seismol* 11, 15–26. <https://doi.org/10.1007/s10950-006-9024-0>

1059 Reinhardt, L.J., Dempster, T.J., Shroder, J.F., Persano, C., 2007. Tectonic denudation and topographic development
1060 in the Spanish Sierra Nevada. *Tectonics* 26, n/a-n/a. <https://doi.org/10.1029/2006tc001954>

1061 Richards, J.P., 2009. Postsubduction porphyry Cu-Au and epithermal Au deposits: Products of remelting of
1062 subduction-modified lithosphere. *Geology* 37, 247–250. <https://doi.org/10.1130/g25451a.1>

1063 Riding, R., Braga, J.C., Martín, J.M., Sánchez-Almazo, I.M., 1998. Mediterranean Messinian Salinity Crisis:
1064 constraints from a coeval marginal basin, Sorbas, southeastern Spain. *Mar Geol* 146, 1–20.
1065 [https://doi.org/10.1016/s0025-3227\(97\)00136-9](https://doi.org/10.1016/s0025-3227(97)00136-9)

1066 Rodríguez-Fernández, J., Azor, A., Azañón, J.M., 2012. Tectonics of Sedimentary Basins 461–479.
1067 <https://doi.org/10.1002/9781444347166.ch23>

1068 Romagny, A., Jolivet, L., Menant, A., Bessière, E., Maillard, A., Canva, A., Gorini, C., Augier, R., 2020. Detailed
1069 tectonic reconstructions of the Western Mediterranean region for the last 35 Ma, insights on driving
1070 mechanisms. *Bsgf - Earth Sci Bulletin* 191, 37. <https://doi.org/10.1051/bsgf/2020040>

1071 Rosenbaum, G., Lister, G.S., Duboz, C., 2002. Relative motions of Africa, Iberia and Europe during Alpine
1072 orogeny. *Tectonophysics* 359, 117–129. [https://doi.org/10.1016/s0040-1951\(02\)00442-0](https://doi.org/10.1016/s0040-1951(02)00442-0)

1073 Sanz de Galdeano, C.S., Vera, J.A., 1992. Stratigraphic record and palaeogeographical context of the Neogene
1074 basins in the Betic Cordillera, Spain. *Basin Res* 4, 21–36. <https://doi.org/10.1111/j.1365-2117.1992.tb00040.x>

1075 Sanz de Galdeano, C.S.D., Rodríguez-Fernández, J., López-Garrido, A.C., 1985. A strike-slip fault corridor within
1076 the Alpujarra Mountains (Betic Cordilleras, Spain). *Geol Rundsch* 74, 641–655.
1077 <https://doi.org/10.1007/bf01821218>

1078 Sanz de Galdeano, C.S. de, Alfaro, P., 2004. Tectonic significance of the present relief of the Betic Cordillera.
1079 *Geomorphology* 63, 175–190. <https://doi.org/10.1016/j.geomorph.2004.04.002>

1080 Scotney, P., Burgess, R., Rutter, E.H., 2000. 40Ar/39Ar age of the Cabo de Gata volcanic series and displacements
1081 on the Carboneras fault zone, SE Spain. *J Geol Soc London* 157, 1003–1008.
1082 <https://doi.org/10.1144/jgs.157.5.1003>

1083 Sosson, M., Morrillon, A.-C., Bourgois, J., Féraud, G., Poupeau, G., Saint-Marc, P., 1998. Late exhumation stages
1084 of the Alpujarride Complex (western Betic Cordilleras, Spain): new thermochronological and structural data on
1085 Los Reales and Ojen nappes. *Tectonophysics* 285, 253–273. [https://doi.org/10.1016/s0040-1951\(97\)00274-6](https://doi.org/10.1016/s0040-1951(97)00274-6)

1086 Spakman, W., Wortel, R., 2004. The TRANSMED Atlas. The Mediterranean Region from Crust to Mantle 31–52.
1087 https://doi.org/10.1007/978-3-642-18919-7_2

1088 Spakman, W., Chertova, M.V., Berg, A. van Hinsbergen, D.J.J., 2018. Puzzling features of western Mediterranean
1089 tectonics explained by slab dragging. *Nat Geosci* 11. <https://doi.org/10.1038/s41561-018-0066-z>

1090 Stich, D., Serpelloni, E., Mancilla, F. de L., Morales, J., 2006. Kinematics of the Iberia–Maghreb plate contact from
1091 seismic moment tensors and GPS observations. *Tectonophysics* 426, 295–317.
1092 <https://doi.org/10.1016/j.tecto.2006.08.004>

1093 Tenedor-Salmerón, V., Galindo-Zaldivar, J., d’Acremont, E., Catalán, M., Martos, Y.M., Ammar, A., Ercilla, G.,
1094 2022. New insights on the Alboran Sea basin extension and continental collision from magnetic anomalies
1095 related to magmatism (western Mediterranean). *Mar Geol* 443, 106696.
1096 <https://doi.org/10.1016/j.margeo.2021.106696>

1097 Teyssier, C., Tikoff, B., 1998. Strike-slip partitioned transpression of the San Andreas fault system: a lithospheric-
1098 scale approach. *Geological Soc Lond Special Publ* 135, 143–158. <https://doi.org/10.1144/gsl.sp.1998.135.01.10>

1099 Vacherat, A., Mouthereau, F., Pik, R., Bellahsen, N., Gautheron, C., Bernet, M., Daudet, M., Balansa, J., Tibari, B.,
1100 Jamme, R.P., Rada, J., 2016. Rift-to-collision transition recorded by tectonothermal evolution of the northern
1101 Pyrenees. *Tectonics* 35, 907–933. <https://doi.org/10.1002/2015tc004016>

1102 van Hinsbergen, D.J.J., Vissers, R.L.M., Spakman, W., 2014. Origin and consequences of western Mediterranean
1103 subduction, rollback, and slab segmentation. *Tectonics* 33, 393–419. <https://doi.org/10.1002/2013tc003349>

Deleted: Pourhiet, L.

Moved up [3]: L. Huet, B., May, D.A., Labrousse, L., Jolivet, L., 2012. Kinematic interpretation of the 3D shapes of metamorphic core complexes: 3D SHAPES OF MCCs. *Geochem Geophys Geosystems* 13. <https://doi.org/10.1029/2012gc004271>

Deleted: ¶

Deleted: <https://doi.org/10.1002/2013tc003349>

1112 Vázquez, M., Jabaloy, A., Barbero, L., Stuart, F.M., 2011. Deciphering tectonic- and erosion-driven exhumation of
1113 the Nevado-Filábride Complex (Betic Cordillera, Southern Spain) by low temperature thermochronology:
1114 Deciphering tectonic- and erosion-driven exhumation. *Terra Nova* 23, 257–263. [https://doi.org/10.1111/j.1365-](https://doi.org/10.1111/j.1365-3121.2011.01007.x)
1115 [3121.2011.01007.x](https://doi.org/10.1111/j.1365-3121.2011.01007.x)
1116 Vergés, J., Fernández, M., 2012. Tethys–Atlantic interaction along the Iberia–Africa plate boundary: The Betic–Rif
1117 orogenic system. *Tectonophysics* 579, 144–172. <https://doi.org/10.1016/j.tecto.2012.08.032>
1118 Vernant, P., Fadil, A., Mourabit, T., Ouazar, D., Koulali, A., Davila, J.M., Garate, J., McClusky, S., Reilinger, R.,
1119 2010. Geodetic constraints on active tectonics of the Western Mediterranean: Implications for the kinematics and
1120 dynamics of the Nubia-Eurasia plate boundary zone. *J Geodyn* 49, 123–129.
1121 <https://doi.org/10.1016/j.jog.2009.10.007>
1122 Villasenor, A., Chevrot, S., Harnafi, M., Gallart, J., Pazos, A., Serrano, I., Córdoba, D., Pulgar, J.A., Ibarra, P.,
1123 2015. Subduction and volcanism in the Iberia–North Africa collision zone from tomographic images of the
1124 upper mantle. *Tectonophysics*. <https://doi.org/10.1016/j.tecto.2015.08.042>
1125 Waldner, M., Bellahsen, N., Mouthereau, F., Bernet, M., Pik, R., Rosenberg, C.L., Balvay, M., 2021. Central
1126 Pyrenees Mountain Building: Constraints From New LT Thermochronological Data From the Axial Zone.
1127 *Tectonics* 40. <https://doi.org/10.1029/2020tc006614>
1128 Weijermars, R., Roep, Th.B., Eeckhout, B.V. den, Postma, G., Kleverlaan, K., 1985. Uplift history of a Betic fold
1129 nappe inferred from Neogene-Quaternary sedimentation and tectonics (in the Sierra Alhamilla and Almería,
1130 Sorbas and Tabernas Basins of the Betic Cordilleras, SE Spain). *Geologie en Mijnbouw* 397–411.
1131 Zeck, H.P., Monié, P., Villa, I.M., Hansen, B.T., 1992. Very high rates of cooling and uplift in the Alpine belt of the
1132 Betic Cordilleras, southern Spain. *Geology* 20, 79. [https://doi.org/10.1130/0091-](https://doi.org/10.1130/0091-7613(1992)020<0079:vhroca>2.3.co;2)
1133 [7613\(1992\)020<0079:vhroca>2.3.co;2](https://doi.org/10.1130/0091-7613(1992)020<0079:vhroca>2.3.co;2)
1134

